Czech Technical University in Prague
Faculty of Electrical Engineering

Department of Cybernetics

BACHELOR PROJECT ASSIGNMENT

Student: Andrey C h i r t s o v

Study programme: Cybernetics and Robotics

Specialisation: Robotics

Title of Bachelor Project: Magnetic Position Sensor

Guidelines:

Propose and implement a position sensor of the pneumatic piston using integrated Fluxgate sensors.
Optimize the sensor parameters by the FEM simulation, verify the achievable precision.

Bibliography/Sources:

[1] E.Herceg: Taking a position on Hydraulic Sensors, Jul 2015
[2] P. Ripka: Magnetic sensors and magnetometers, Artech House, London, UK, 2001
[3] T.Reininger, F.Welker, M. von Zeppelin: Sensors in position control applications for industrial automation, Cardiff, UK 4-6 July 2004

Bachelor Project Supervisor: prof. Ing. Pavel Ripka, CSc.

Valid until: the end of the summer semester of academic year 2017/2018

L.S.

prof. Dr. Ing. Jan Kybic
Head of Department

prof. Ing. Pavel Ripka, CSc.
Dean

Prague, January 14, 2017

Bachelor thesis

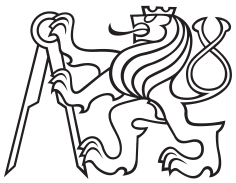

Czech Technical University in Prague

F3

Faculty of Electrical Engineering
Department of Cybernetics

Magnetic position sensor

Andrey Chirtsov

Supervisor: prof. Ing. Pavel Ripka, CSc.
May 2017

Acknowledgements

I want to express my gratitude to Prof. Pavel Ripka for choosing the right directions in this work, for comments on the work that significantly improved this thesis, for a lot of time for discussing. I also want to express my acknowledgement to Ing. Jan Vyhnánek for the patient explanation of technical issues and for helping to create this work. I also thank Vaclav Grim for assistance with a FEM simulation and my family for their support.

Declaration

I declare that the presented work was developed independently and that I have listed all sources of information used within it in accordance with the methodical instructions for observing the ethical principles in the preparation of university theses.

Prague, May 16, 2017

Prohlašuji, že jsem předloženou práci vypracoval samostatně, a že jsem uvedl veškeré použité informační zdroje v souladu s Metodickým pokynem o dodržování etických principů při přípravě vysokoškolských závěrečných prací.

V Praze, 16. května 2017

Abstract

Position sensors have always been widely demanded in the industry. These sensors are necessary for control, monitoring, diagnostics of pneumatic and hydraulic cylinders. Today the most common method for measuring the piston is the permanent magnet mounted on the end of the piston rod, and the array of Hall sensors mounted on the surface of the cylinder.

The purpose of this work is to design the magnetic position sensor which measures a position of a piston in pneumatic cylinders without permanent magnet using integrated Fluxgate sensors DRV425EVM.

Keywords: position sensor, Fluxgate, DRV425, magnetic sensor, pneumatic cylinder

Supervisor: prof. Ing. Pavel Ripka, CSc.

Abstrakt

Polohové senzory byly vždy hojně využívány napříč celým průmyslem. Jsou nezbytné pro řízení, kontrolu a diagnostiku pneumatických a hydraulických válců. Dnes nejrozšířenějším způsobem měření pozice pístu je permanentní magnet, který je umístěný na konci pístnice a řada Hallových senzorů připevněná na povrch válce.

Cílem této práce je návrh magnetického polohového senzoru, který bude snímat umístění pístu v pneumatických válcích bez permanentního magnetu využívaje integrované Fluxgate sensory DRV425EVM.

Klíčová slova: senzor polohy, magnetický senzor, pneumatický válec, DRV425, Fluxgate

Contents

Figures

Tables

Chapter 1

Introduction

1.1 About pneumatics cylinders

Pneumatic cylinders are used in all industries where it is necessary to perform translational movements. Pneumatic cylinders are found in press production, filling and packaging lines of products, in the structure of vehicles, in lifts and conveyor systems. Thanks to the use of compressed air and not oil, as in hydraulic cylinders, pneumatic tubes are becoming more common in many areas of industry and the national economy, as cheap mechanisms that do not require expensive maintenance and scarce spare parts.

Many directional-control valves are rated for a maximum pressure of 680 kPa to 860 kPa. Using them, we can produce thousands of Newtons over a broad range of velocities; cycle at high speeds without overheating, and stall without internal damage. Pneumatic cylinders are simple, durable, quiet and easy to install. They also easily endure harsh conditions such as high humidity, dusty environment, and repeated high-pressure wash downs.[1] As shown in Figure 1.1, the pneumatic cylinder consists of 3 main parts: piston rod, piston, and tube.

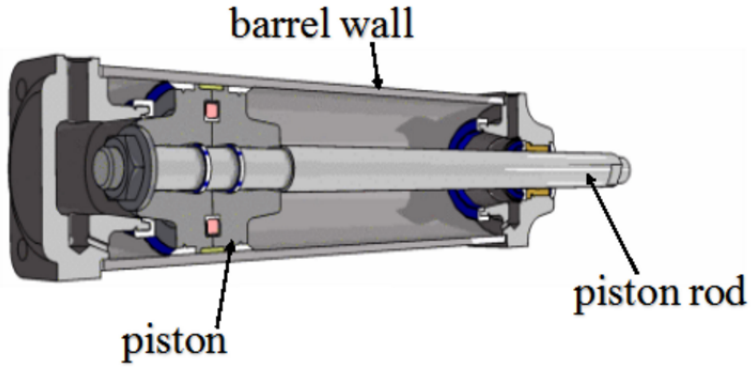

Figure 1.1: Main parts of the pneumatic cylinder [2]

The piston is a disc or cylinder at the end of a rod; the piston rod transfers the force it develops to object to being moved. Tubes that are used in pneumatic cylinders have a non-ferromagnetic body, and in general they are

made of aluminum or carbon fiber reinforced polymer or simply called carbon fiber, that is an extremely strong material. The non-ferromagnetic body of pneumatic cylinders tube allows us to measure the position in a non-contact way using the magnetic field. On the contrary in hydraulic cylinders instead of aluminum or carbon fiber, steel is used which is ferromagnetic, it does not allow us to use an embedded permanent magnet because its magnetic field is shielded by the steel walls of the tube.

Position sensors have always been widely demanded in the industry. These sensors are necessary for control, monitoring, diagnostics of pneumatic and hydraulic cylinders.

1.2 Computing Pneumatic Cylinder Force

1.2.1 Single-acting cylinder

The single acting cylinder uses air or specific aerosol pressure to provide the force only in one direction, and spring tension or gravity to provide the force in the opposite direction. Figure 1.2 shows a single-acting cylinder. The force

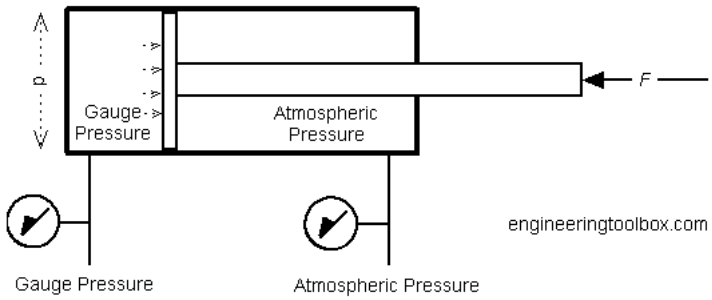

Figure 1.2: Single-acting cylinder [4]

exerted by a single acting pneumatic cylinder can be expressed as shown in Equation 1.1.

$$F = pA = p\frac{\pi d^2}{4} \tag{1.1}$$

where
F = force exerted, (N)
p = gauge pressure, $(N/m^2, Pa)$
A = full bore area, (m^2)
d = full bore piston diameter, (m)

But it must be taken into the account that the force exerted would be on the push stroke only and not on the retraction end of the cylinder. The diameter of the push rod must be subtracted from the overall area, as the connection of the push rod interferes with the force measurement. This statement applies to both single-acting cylinder and double-acting cylinder.

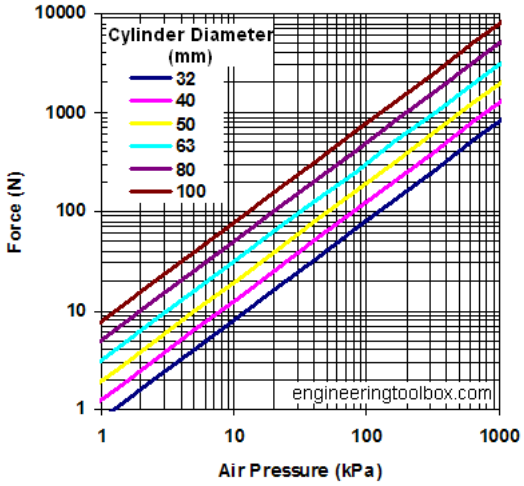

Figure 1.3: Force as the function of the air pressure in pneumatic cylinders [4]

1.2.2 Double-acting cylinder

Most piston type actuating cylinders are double-acting, which means that air under pressure can be applied to either side of the piston to apply force and provide movement. They have two ports to allow air in, one for outstroke and one for instroke. Stroke length for this design is not limited. However, the piston rod is more vulnerable to buckling and bending. Additional calculations should be performed as well.[3] Figure 1.4 shows a double-acting cylinder.

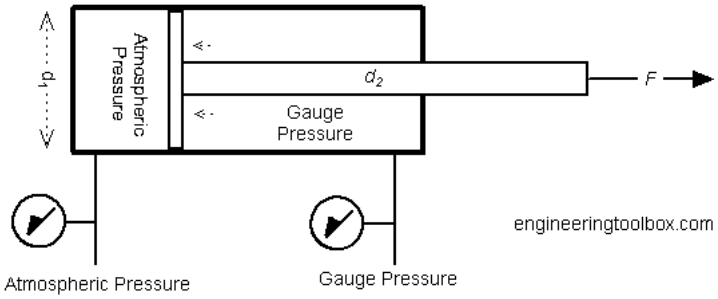

Figure 1.4: Double-acting cylinder [4]

The force exerted by double acting pneumatic cylinder on outstroke can be expressed by Equation 1.1. The force exerted on instroke can be expressed by Equation 1.2.

$$F = p\pi \frac{(d_1^2 - d_2^2)}{4} \tag{1.2}$$

where

d1 = full bore piston diameter, (m)

d2 = piston rod diameter, (m)

1.3 Stroking speed of a pneumatic cylinder

Speed affects productivity, longevity, and controllability. We can calculate the approximate stroking speed of a pneumatic cylinder from Equation 1.3 [1]:

$$s = \frac{q}{A} \tag{1.3}$$

where
s = speed, (m/s)
q = airflow, (m^3/s)
A = piston area, (m^2)

Other factors that might affect speed include port sizes, inlet, and exhaust flow through control valves, and hose or tubing sizes — if they create bottlenecks that restrict air flow to or from the cylinder. Likewise, air pressure that is barely capable of moving the load will hamper speed.

With any fixed combination of valve, cylinder, pressure, and load, it is usually necessary to have adjustable control over cylinder speed. Flow controls at the cylinder ports let users tune speed to their application.

For most applications, unidirectional flow regulators installed to restrict flow out of the cylinder and permit free flow in giving the best results. A regulator in the rod-end port controls extension speed, and one on the cap-end port controls retraction. [1]

1.4 State of the art

At present, there are three conventional methods of measuring the position of the piston in the cylinder: magnetostrictive, variable resistance, and variable inductance sensors.[5]

Drawback of a magnetostrictive method which uses a ring-shaped permanent magnet embedded in the piston is the cost, the need for drilling a small diameter blind hole into the internal end of the cylinder rod, so-called "gun drilling" because it looks like a gun barrel and also non-universality because most magnetostrictive-sensor manufacturers have own style of permanent magnet with proprietary mounting features, such the number of holes, the hole pattern, etc.

The disadvantage of a variable resistance (potentiometer-type) method is the need for insulated round carrier, which is attached to the internal end of the gun-drilled cylinder rod, they also undergo wear which limits service time, particularly if pneumatic or hydraulic cylinder works at high frequencies, or even more importantly, dithered over a short range to improve a system's dynamic characteristics. Because a resistance pot is embedded into the cylinder, replacement of a worn-out pot can be time-consuming and expensive, and may even necessitate replacing the entire cylinder.

The drawback of the variable inductance method is the reliability issue associated with the necessity of the drilling hole in the rod and necessary fitting for the sensor, which resides inside the cylinder.

What is the disadvantage of drilling holes? First of all, this is the mechanical intervention in the construction, which breaks the integrity of the cylinder, then the high cost, the need for specialized equipment, and reliability issues of sensor placement inside the piston rod.

Similar shortcomings have microwave displacement sensors.[6] Vision-based sensors[7] and incremental optical position sensors [8, 9] were also developed but they did not find their industrial application due to reliability problems. Some systems use magnetic scale of a piston rod together with Hall sensors. [10]

We replaced Hall sensors by integrated fluxgate sensors and measured the magnetic field as a function of the passage of the permanent magnet near the sensor for different distances as shown in Figure 1.5. It can be argued based on this results that the sensitivity of sensors can be changed by decreasing or increasing the distance to the magnet or by changing the size of the magnet. The disadvantages of the method in which a permanent magnet is used are influence of the external magnetic fields including those induced by DC currents and the need for non-magnetic stainless steel piston rod, which is expensive.

In this thesis, we will propose a new way of measuring the position of the piston in the pneumatic cylinder without permanent magnet by integrated fluxgate sensors that are more precise and more stable. These sensors provide with an internal compensation coil to support a high-accuracy sensing range of $\pm 2\ mT$. The low-offset, the low crossfield error, that in our case has a significant meaning, offset drift $\pm 5\ nT/°C$, low gain drift and of course one of the main advantages is the low price (3$).[12] Fluxgate sensors have advantages over almost all characteristics in comparison with the sensors that are most commonly used in this field, namely, AMR, GMR and Hall sensors.

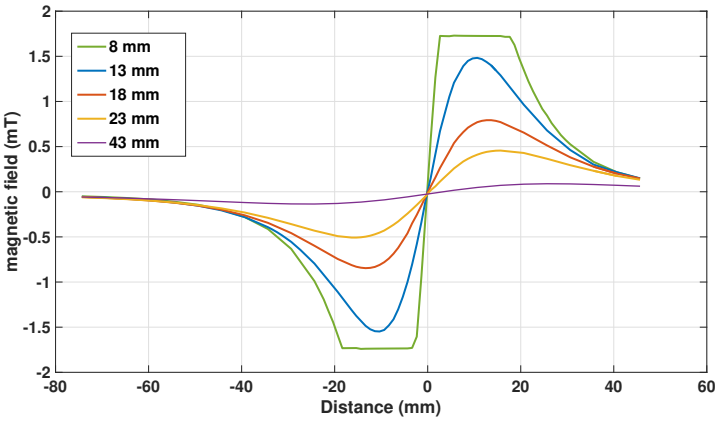

Figure 1.5: Measuring the position of the permanent magnet by integrated fluxgate sensors DRV425

Chapter 2

Suggested new solution

2.1 Our design

In this work, we designed two magnetic methods for detecting piston in the pneumatic cylinder without a permanent magnet. Our technique is based on the magnetic properties of the iron piston rod, and the primary attribute that we use is the high permeability. The iron rod changes the magnetic field as it passes inside the cylinder, and we detect this change in the magnetic field using fluxgate sensors. The main thing is to use the magnetic field of the coils so that their field can penetrate inside the cylinder. To visualize the changes in the magnetic field caused by the iron rod, a FEM simulation was performed and results are shown in Figure 2.1.

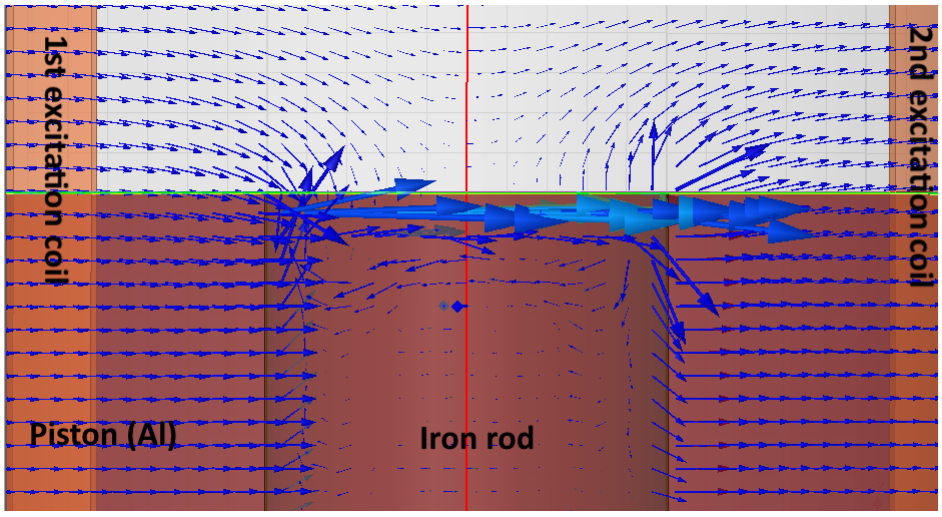

Figure 2.1: Magnetic field vector: FEM simulation for 2 saddle coils - changes in the magnetic field caused by the iron rod, f_{exc}=4 Hz

The first method is using axial coil directly on the cylinder surface as a field source (see Figure 3.5) and the second method is using two saddle coils that are connected in series (see Figure 5.2). The serious problem is that our barrel wall is electrically conducting and causes significant attenuation of the magnetic field of the coil, so we need to find the correct excitation frequency

of the coils so that the electromagnetic field penetrates into the pneumatic cylinder. It is evident that this frequency must be sufficiently small. All parameters including the length and diameter of the cylinder and piston rod, wall thickness, which we used in our model are close to real ones which were taken from the website of the company "Stransky a Petrzik" [11] that produces and develops pneumatic components. We used an aluminum tube as it has the same magnetic properties (mainly relative permeability μ_r=1), piston made of aluminum and piston rod made of steel. The dimensions of the parts are described in Table 2.1.

Part of the pneumatic cylinder	Size (mm)
Pipe diameter	60
Pipe length	500
Barellwall thickness	2
Aluminum piston thickness	10
Piston rod diameter	20
Piston rod length	700

Table 2.1: Parameters of the experimental model

2.2 Depth of penetration

Penetration depth is a measure of how deep the field (E, D, B, H, J) can penetrate into the material. It is defined as the depth at which the intensity of the radiation inside the material falls to 1/e (about 37%) of its original value at (or more correctly, just beneath) the surface. When electromagnetic radiation is incident on the surface of material, it may be (partly) reflected from that surface, and there will be a field containing energy transmitted into the material.This electromagnetic field interacts with the atoms and electrons inside the material. Depending on the nature of the material, the electromagnetic field might travel very far into the material or may die out very quickly. [13]

2.2.1 Beer-Lambert Law

$$I(z) = I_0 e^{-az} \tag{2.1}$$

from the Beer-Lambert law (2.1), we see that the intensity of electromagnetic waves falls in an exponential form. Penetration depth is denoted δ and is given as $\delta = \frac{1}{\alpha}$, but especially for conductors apply to this equation:

$$\delta = \frac{1}{\alpha} = \sqrt{\frac{2}{\omega\mu\sigma}} \tag{2.2}$$

where
ω = angular frequency of current = $2\pi \times frequency$, (rad/s)

μ_r = relative magnetic permeability of the conductor
μ_0 = the permeability of free space, H/m
$\mu = \mu_0\mu_r$
σ = electrical conductivity, S/m

	Frequency (Hz) **Material at 20 ° C**	**10**	**50**	**100**	**1000**	**10 000**	**1 000 000**
$\delta(mm)$	Copper	20.6	9.21	6.52	2.06	0.65	0.065
	Aluminum	26.9	12.03	8.51	2.69	0.85	0.085
	Carbon steel (1010) at 0.002 T	6.01	2.69	1.9	0.6	0.19	0.019

Table 2.2: Frequency dependence at penetration depth for 3 different materials

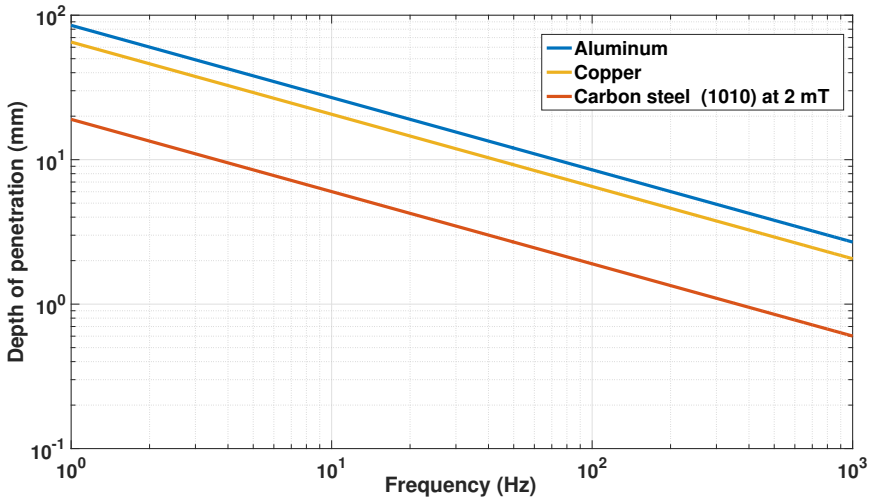

Figure 2.2: Frequency dependence of the penetration depth for 3 different materials up to 1 kHz

2.3 Fluxgate sensors

The main question that interests many, why did we choose the fluxgate sensors?

Hall-effect sensors are most common in magnetic field sensing, but their lower sensitivity, offset and offset drift with temperature, noise, gain variation, and nonlinearity limits the achievable resolution and accuracy of the system. In comparison with AMR sensors, their main drawback is that they have a small range (0.2 mT), which will be insufficient for this application and also completely failed if the perpendicular magnetic field, so-called crossfield is stronger than their full-scale range, since their single domain state will be broken and in order for the sensor to be again suitable for use, it needs to be magnetized. Fluxgate sensors offer significantly higher sensitivity, lower drift, lower noise, and high linearity and enable up to 1000-times better accuracy of the measurement. These characteristics make the fluxgate sensor uniquely

suited for high-performance magnetic-field sensors and applicable in many industrials areas.

Fluxgate sensors measure the magnitude and direction of the DC and low-frequency AC magnetic field in the range of approximately 10^{-10} to 10^{-4} T. The soft magnetic material of the sensor core is periodically saturated in both polarities by the AC excitation field, which is produced by the excitation current I_{exc} through the excitation coil. Because of that, the core permeability changes, and the dc flux associated with the measured dc magnetic field is modulated; the "gating" of the flux that occurs when the core is saturated gave the device its name. The device output is usually the voltage V_I induced into the sensing (pickup) coil at the second (and also higher even) harmonics of the excitation frequency. This voltage is proportional to the measured field.[14]

2.3.1 DRV425 Functional Block Diagram

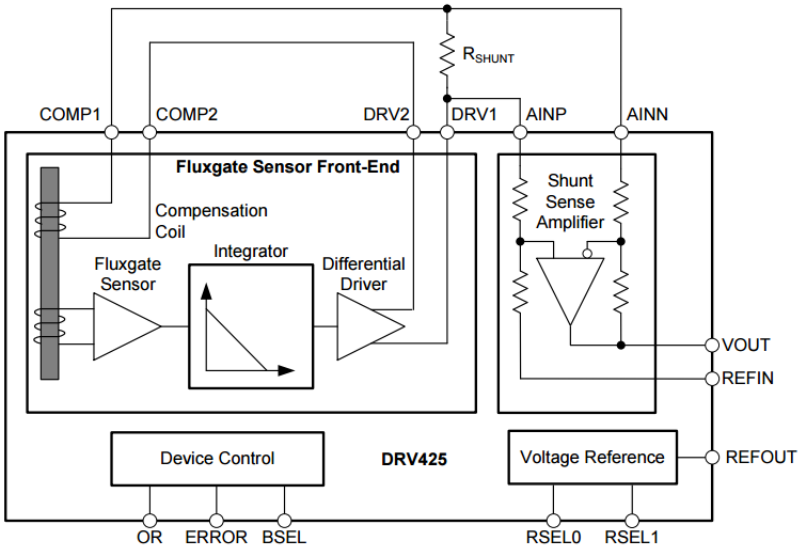

Figure 2.3: Functional Block Diagram [12]

As shown in Figure 2.3, the DRV425 consists of a magnetic fluxgate sensor with the necessary sensor conditioning and compensation coil to internally close the control loop. The fluxgate sensor is repeatedly driven in and out of saturation and supports hysteresis-free operation with excellent accuracy. The internal compensation coil assures stable gain and high linearity. The magnetic field (B) is detected by the internal fluxgate sensor in the DRV425. The device integrates the sensor output to assure high-loop gain. The integrator output connects to the built-in differential driver that drives an opposing compensation current through the internal compensation coil. The compensation coil generates an opposite magnetic field that brings the original magnetic field at the sensor back to zero. The compensation current

is proportional to the external magnetic field, and its value is 12.2 mA/mT. This compensation current generates a voltage drop across an external shunt resistor, R_{SHUNT}. An integrated differential amplifier with a fixed gain of 4 V/V measures this voltage and generates an output voltage that is referenced to REFIN and is proportional to the magnetic field. The value of output voltage at the VOUT pin (VVOUT) is calculated using Equation 2.3 [12]

$$V_{VOUT}[V] = B \cdot G \cdot R_{shunt} \cdot G_{AMP} = B[mT] \cdot 12.2mA/mT \cdot R_{shunt}[\Omega] \cdot 4[V/V] \tag{2.3}$$

2.3.2 Crossfield error

The benefit of our fluxgate sensors is that they have a low crossfield error. Crossfield effect (or crossfield error) is unwanted sensitivity to the field which is orthogonal to the sensing direction of the magnetic sensor. It may cause serious errors of sensor systems, e.g. navigation devices or multichannel gradiometers for location and recognition of ferromagnetic objects. [15]. It is shown in Figure 2.4 that crossfield error on our sensor range is in the interval from -1.5 μT to 0.3 μT, which is only 0.3% of the full-scale range. This benefit we will use in our measurement.

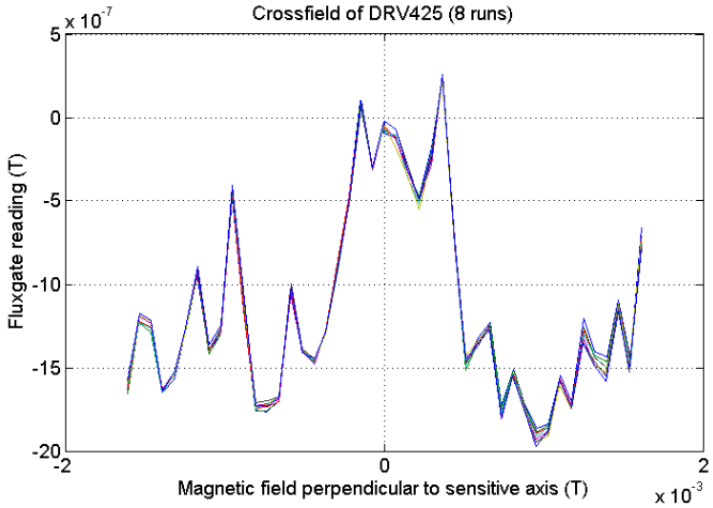

Figure 2.4: DRV425: linearity error as the function of the crossfield effect[16]

2.4 Electrical connection of sensors

For preliminary measurement with one coil wound on a cylinder and the saddle coils, we used only five sensors with a simple connection to the Lock-In amplifier SR865A. This connection is shown in Figure 2.5, we used two signals, one is the sensor output and the second is its reference signal. The bill of materials that we used is shown in Table 2.3.

C11 is known as a filter capacitor employed in the circuit to stabilize the slow alterations in the output voltage of the voltage stabilizer 7805. Moreover, this capacitor is not alone capable of suppressing very short spikes at the output.

C12 is the filter capacitor employed to stabilize the slow changes in the voltage applied to the input of the voltage stabilizer.

C33 and C34 is known as bypass capacitor and worked to bypass very short period spikes to the ground with no influence the other components.

LED diode D1 serves to indicate that the circuit is switched on.

D2 blocks all current flowing in the reverse direction.

R2 limits the current flowing through the LED diode D1.

U12, U13, U14, U15, U16 are magnetic sensors DRV425, which measure one component of the magnetic field.

U17 is the voltage regulator, which at its output gives a reference voltage 5 V. This voltage is needed to power our sensors.

DESIGNATORS	DESCRIPTION
D1	LED, Green, 2.1 V, 3 mm, 60°, 12.6 mcd at 10 mA
D2	Diode, 600 V/1 A, DO41, Uf= 1.2V, trr= 200 ns
R2	RES, 910, 1%, 0.6 W, 0207
U12, U13, U14, U15, U16	Fluxgate sensor DRV425 Evaluation Module
U17	7805 5V Voltage Regulator, TO-220
C11,C12	CAP, POL, 22 uF, 25 V, ± 20%, SIZE 5x11 mm
C33,C34	CAP, CERM, 100 nF, 63 V, +80%/-20%, Y5V
P1,P2,P3,P4,P5,P6	Header, 100 mil, 2x1, Copper Alloy, Straight, TH

Table 2.3: Bill of materials for connection with 5 sensors

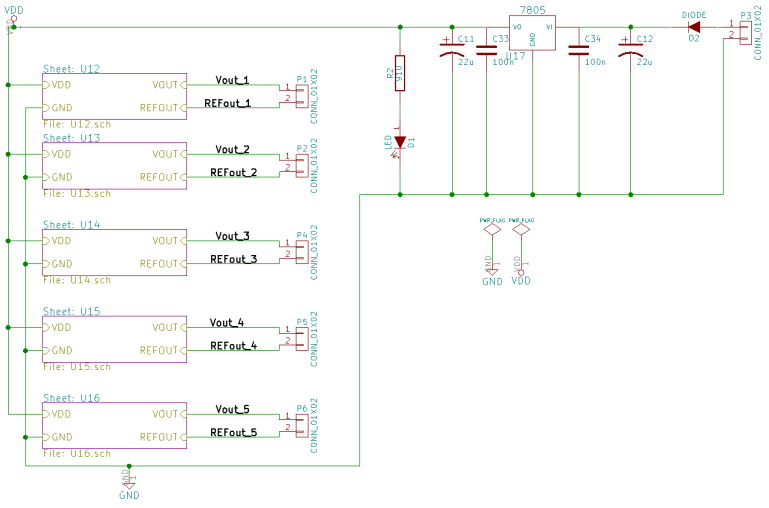

Figure 2.5: Connection of 5 sensors

For both cases, the general connection of the sensors was as shown in Figure 2.6. The connection of the sensors was taken from the datasheet DRV425EVM

and will be described in Subsection 2.4.1. Based on these measurements, we designed PCB with 16 sensors and used a connection to a computer through a multifunctional I/O device NI USB-6212 where we read all the information from the magnetic sensors and the reference position potentiometric sensor.

The maximum field measurement range in our case is $\pm$ 500 μT because of the used shunt resistor $R_{shunt} = 100\ \Omega$, but the maximum magnetic field range of the DRV425 is $\pm 2\ mT$. To increase the sensitivity, R_{shunt} can be adjusted based on Equation 2.4. [12]

$$B = \frac{V_{out}}{G \cdot G_{fg} \cdot R_{shunt}} \tag{2.4}$$

Higher magnetic fields result in increased current flowing through R_{shunt}. The output voltage of the differential amplifier in the DRV425 will reach its peak amplitude with a maximum voltage drop across R_{shunt} as shown in Equation 2.5.

$$VR_1 = \frac{VDD - REFOUT}{4} \tag{2.5}$$

2.4.1 Sensor wiring diagram

The electrical circuit of the sensor connection that was taken from the datasheet DRV425EVM is shown in Figure 2.6. The bill of materials of the evaluation module is in the Table 2.4. R_2 and R_9 are 10-$k\Omega$ pull-up resistors on the Over Range (/OR) and Error (/ER) flag output pins respectively. These outputs are open drain and a pull up is required to observe the active low output state. These pins may also be wired to a microcontroller for use as interrupt pins. Our magnetic sensors in both cases are powered by 5 V, which is obtained by using the IC voltage regulator 7805. But it should be noted that this regulator has 2 V linear drop-out. That means we must give it at least 7 V to get a clean 5 V out. There is a constant 'quiescent' current draw of 6 mA.

DESIGNATORS	DESCRIPTION
C1,C2	CAP, CERM, 1 μF, 25 V, $\pm$ 10%, X7R, 0603
J1	Header, 100mil, 4×1, Gold, R/A, TH
R1	RES, 100, 1%, 0.125 W, 0805
R2, R9	RES, 10 k, 5%, 0.063 W, 0402
R3, R5, R7	RES, 0, 5%, 0.05 W, 0201
U1	Fluxgate Magnetic Field Sensor
R4, R6, R8	Not Installed

Table 2.4: Bill of Materials DRV425EVM [12]

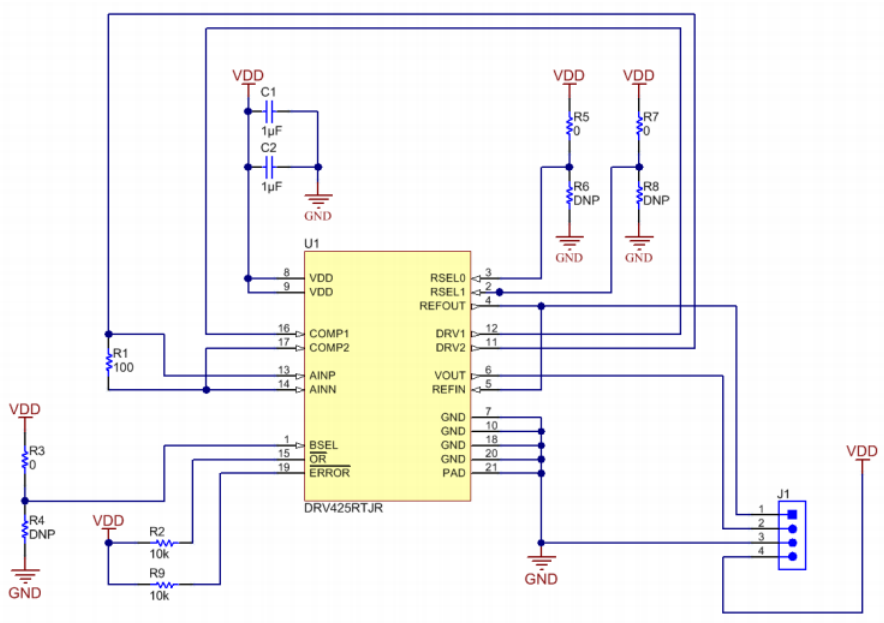

Figure 2.6: DRV425 Evaluation Module Schematic [12]

2.4.2 Equation for transferring sensor voltage to magnetic field strength

From the Figure 2.7, 2.8, we see that the output voltage as the function of the magnetic field is linear and the maximum error is approximately 0.1% at 200 mT which is negligible for our application. We can compose the equation for transferring the output sensor voltage V_{out} to the magnetic field B_m:

$$B_m(\mu T) = \frac{V_{out}(mV)}{5} \tag{2.6}$$

To compare the measured results and the results of the simulation, we also use magnetic field intensity or strength H (A/m). It is defined by Equation 2.7, and we know that in air relative permeability $\mu_r = 1$ and $\mu_0 = 4\pi \cdot 10^{-7}$ H/m.

$$H = \frac{B_0}{\mu_0 \mu_r} \tag{2.7}$$

The relation between the sensor output V_{out} (mV) and H (A/m) can be described by Equation 2.8.

$$H(A/m) = \frac{V_{out}(mV)}{2\pi} \tag{2.8}$$

2.5 Potentiometric reference position sensor

For verifying the accuracy of the measurement, we used a potentiometric linear position sensor MRTM500 with a measurement range of 500 mm and

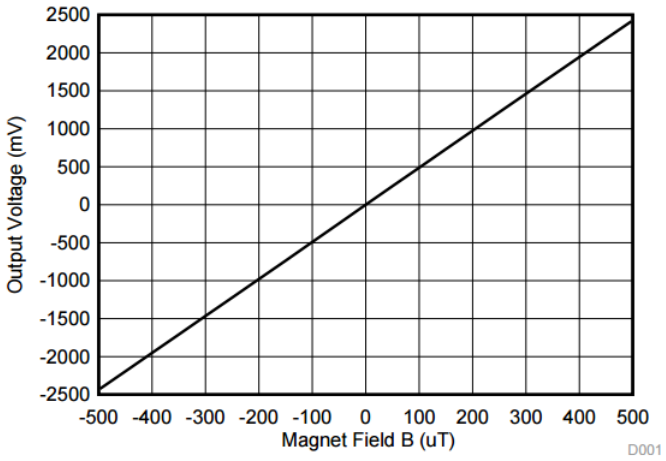

Figure 2.7: Output Voltage vs. Magnetic Field Strength [12]

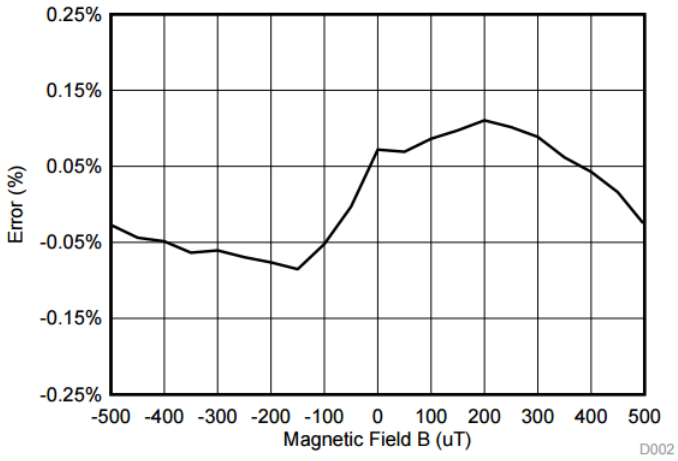

Figure 2.8: Error vs. Magnetic Field Strength [12]

resistance 5 $k\Omega$. How this sensor looks like is shown in Figure 2.9. The linearity error of the sensor is 0.05%. The reference sensor slider is attached to the iron rod using a thread bolt. Using a multimeter, we can read the changing resistance of the potentiometric sensor, but it has the main drawback that the resistance varies with temperature. This can be caused both by self-heating of the resistor by the passage of current and by changing the ambient temperature. To avoid this effect, we use a potentiometric connection as shown in Figure 2.10 and read output voltage V_{out} of the reference sensor.

For the exact reference voltage, we used the adjustable micropower voltage regulator LP2951. This circuit is suitable for use in battery-powered applications because it has low quiescent current, low dropout voltage, and low temperature coefficient. We can adjust the resistors R_1, R_2 for the output reference voltage 4 V by Equation 2.9 taken from the datasheet. Capacitor

Figure 2.9: Potentiometric reference sensor [19]

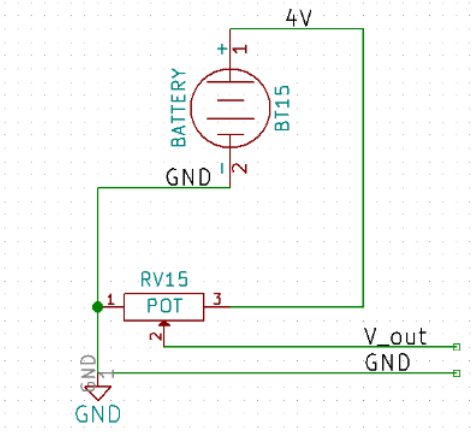

Figure 2.10: Electrical connection of the potentiometric sensor

Co is required between the output and ground for stability at output voltages. Since I_{FB} is controlled to less than 40 nA, the error associated with this term is negligible in most applications. For the output voltage 4 V, we calculated R_1=22 $k\Omega$ and R_2=10 $k\Omega$, V_{ref} is taken from the datasheet and equals 1.26 V.

$$V_{out} = V_{ref}(1 + \frac{R_1}{R_2}) + I_{FB}R_1 \tag{2.9}$$

Chapter 3

Axial coil sensor

The first method with which we began to work is an axial coil sensor. For this case, the magnetic field was measured by an array of sensors consisting of 5 DRV425EVM. A coil was wound on a cylinder using 808 turns of copper wire with the diameter of 0.56 mm, in such a way that the magnetic field is co-directed with the main axis of the cylinder. The coil was excited by a functional generator KEITHLEY 3390 with an internal resistance of 50 Ω. The RMS voltage was V_{RMS}=1.6 V and the current flowing through the coil was dependent on the excitation frequency of this coil, for example for $f_{exc} = 50$ Hz, the RMS current was I=105.84 mA and for f_{exc} =1 kHz the RMS current was 99 mA. The characteristics of the coil, namely its inductance and resistance at different excitation frequencies are given in Table 3.1. To know the magnetic field inside the cylinder we measured it with a sensor in two positions: in the middle of the cylinder and at its end. The dependence of the magnetic field on the exciting frequency from 10 Hz to 10 kHz is shown in Figure 3.1. As expected, the dependence has an exponential form and completely corresponds to Beer-Lambert Law (Subsection 2.2.1). In the middle of the cylinder at a frequency 10 Hz, the intensity of the magnetic field is 156 A/m, at the same frequency, but at the end of the cylinder, the intensity is 120 A/m. The data we measured are corresponding to the theoretical value of 151 A/m, which was obtained from equation $H = \frac{NI}{L}$. The field measured at the and of the coil was higher than the theoretical value due to the eddy currents. We repeated the same measurement at DC and measured value in the middle of the cylinder was 163 A/m and at the end it was 87 A/m. The field at the end decreases to 50 % as theoretically predicted.

	DC	**AC 100 Hz**	**AC 1 kHz**
L(mH)	-	3.49754	0.3864
R(Ω)	14.1	15.4835	18.5481

Table 3.1: Parameters of axial coil

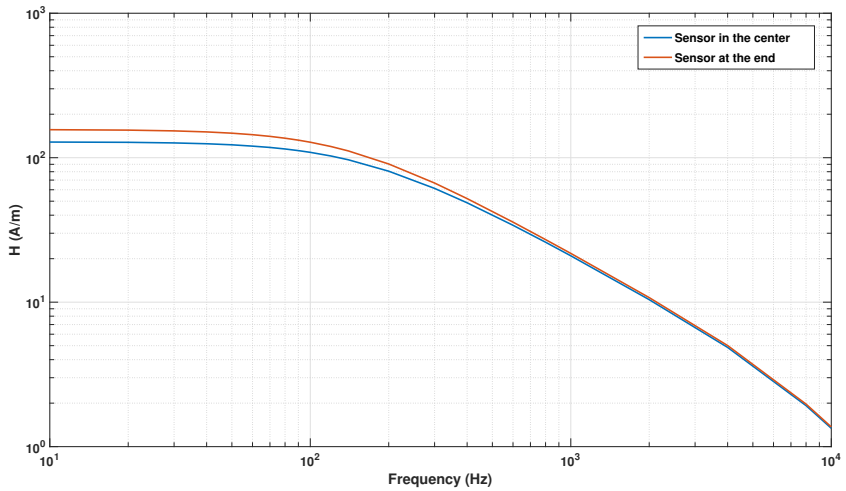

Figure 3.1: Magnetic field inside the cylinder as a function of the excitation frequency

3.1 FEM Simulation

3.1.1 About FEM

The finite element method (FEM) is a numerical method for solving problems of engineering and physics. The finite element method formulation of the problem results in a system of algebraic equations. The method yields approximate values of the unknowns at a discrete number of points over the domain. To solve the problem, it subdivides a large problem into smaller, simpler parts that are called finite elements. The simple equations that model these finite elements are then assembled into a larger system of equations that models the entire problem. FEM then uses variational methods from the calculus of variations to approximate a solution by minimizing an associated error function.[17]

3.1.2 Parameters of the simulation

For finding optimal excitation frequency and placement of the sensors, we used the ANSYS Electronic Desktop to perform the simulation using the finite element method (FEM). The model was simulated in the case of excitation from 2 Hz to 128 Hz. The properties of the materials are given in Table 3.2. The simulation was made by Vaclav Grim. The resulting magnetic field for different piston position in axial and radial direction is shown in Figure 3.2. Of course, the magnetic field inside the cylinder is many times larger than outside, but our sensors are quite sensitive, so this does not make us any problems.

The sensitivity decrease with frequency is caused by two effects [18]:

Material	El. conductivity (S/m)	μ_r
The iron rod	10^7	50
The aluminum piston and tube	38·10^6	1.000021

Table 3.2: The properties of the materials in the simulation with the axial coil

1. Eddy currents in the aluminum cylinder: the field from the excitation coil is attenuated by the shielding effect as shown in Figure 3.1, and the response from the rod is attenuated again before it reaches the sensors. These two shielding factors are not the same, as in the first case the attenuated field is in the axial direction, while in the second case it is in the radial direction

2. Eddy currents in the piston bar. They are also the main source of phase shifts.

From the simulation we see that the eddy currents at low frequencies are negligible and we detect the iron rod only by using its permeability.

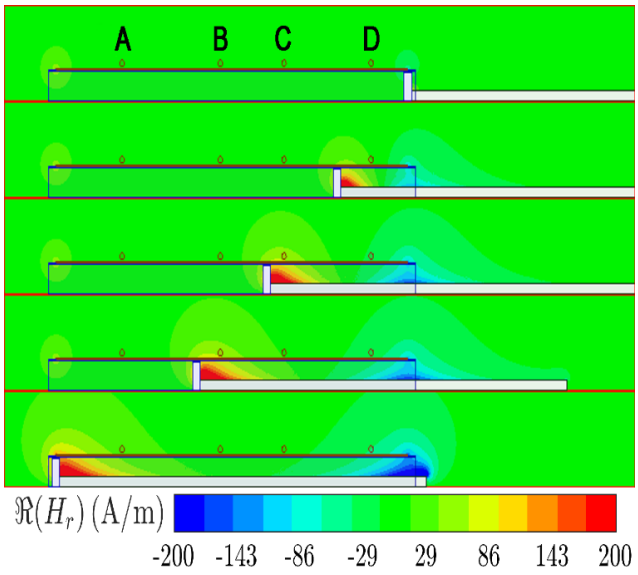

The simulation was calculated for points A, B, C, D and waveforms for these points have similar shape. The simulated reading of the sensor in position B as the function of the piston position is shown in Figure 3.3 from the frequencies from 2 Hz to 128 Hz for the real component of the radial direction and we see that at low frequencies it reaches a maximum value in the vicinity of the presence of the piston rod. These results look optimistic; the next step is to make measurements and compare with the results of the simulation.

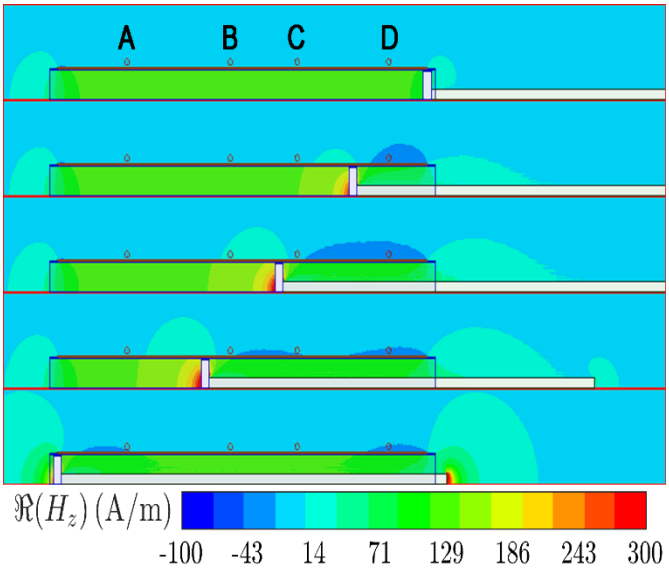

Figure 3.2: FEM simulated field for several positions of the piston: a) radial component and b) axial component. The excitation frequency was 2 Hz. The location of the sensors is marked A to D (simulation by V.Grim)

3.2 Measurement

For verifying the results of the simulation, I performed measurements with the same frequency of excitation for radial and axial direction. As it was written in Subsection 2.3.2, our sensors have a low crossfield error. In that case, it is possible to place the sensors in a radial position in which the magnetic field of the coil will be perpendicular to the sensors without harming the accuracy of the measurements. Holders for our sensors were made on a 3D printer and they allow us to place the sensitive sensor axis directly perpendicular to the cylinder for measuring the radial component of the magnetic field and parallel to the cylinder for measuring the axial component. The 3D model of the sensor holder is shown in Figure 3.4.

The experimental installation is shown in Figure 3.5, the voltage on the sensors is read using a Lock-In amplifier SRS SR865. The reference signal for SRS865 was derived from the coil current. If we measured only the amplitude of the signal, this would not be applicable to the detection of the piston rod.

The results of the measurement are shown in Figure 3.6 for the radial direction of the magnetic field. Results for the real, imaginary component and module are shown in Figure 3.7. It can be seen that in the region when the iron rod passes through the sensor placement, the intensity Hx (real part) has the highest value. The benefit of radial direction in comparison with the axial direction is that it is two times more sensitive, but the axial field response is linear in the vicinity of the sensor location, which can also be used for the position sensing. And in addition to that, the function of the intensity of the magnetic field crosses zero when passing the iron rod as shown in Figure 3.7.

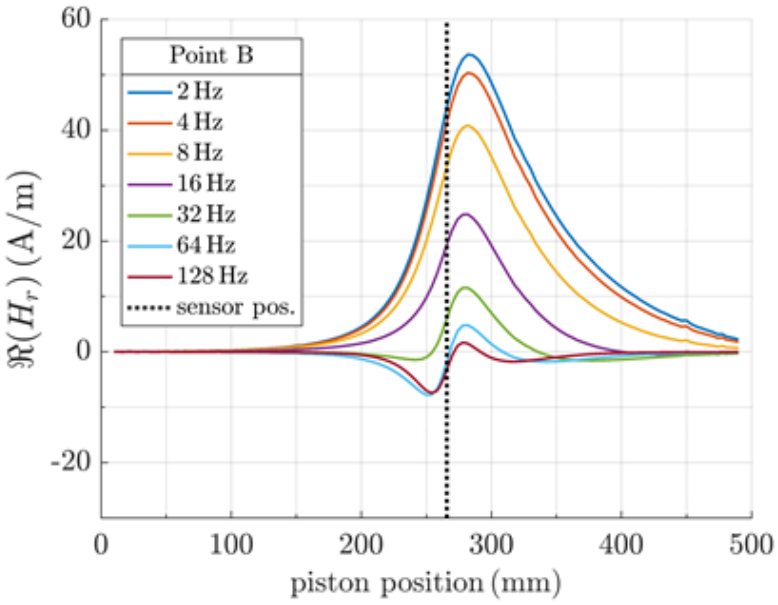

Figure 3.3: The reading of the sensors in positions B as the function of the piston position (simulation by V.Grim)

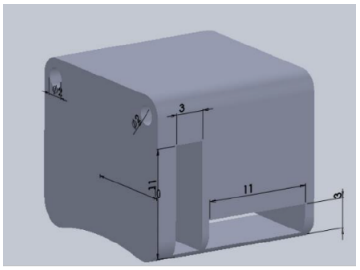

Figure 3.4: The holder for the sensor. 3D model

If we compare the simulation with the measurement results, it is a nice fit, excluding the amplitude value, because of simulations results depend on the permeability of the iron rod. There are also some discrepancies at the higher frequencies because of phase-shifts and the eddy current begin to have the effect. It should be also noted that whole the simulation was made for constant value of the excitation current, the RMS current value during the measurements was changing with frequency from 103 mA to 105 mA.

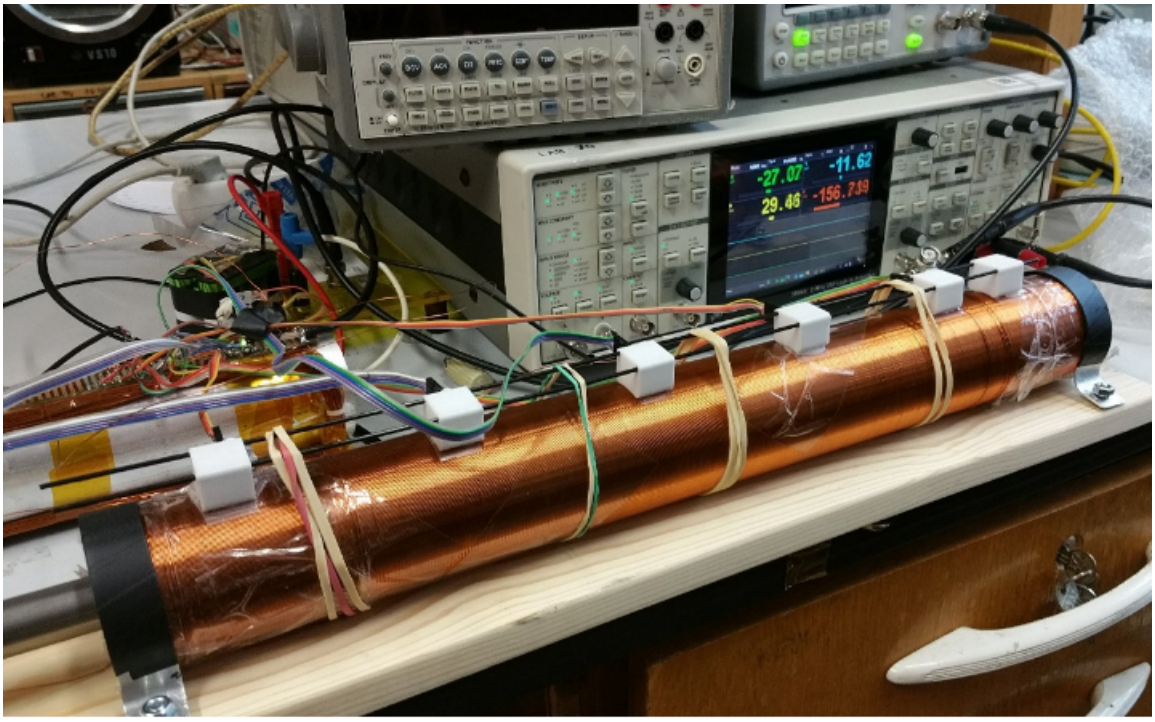

Figure 3.5: Experimental model at the laboratory with axial coil

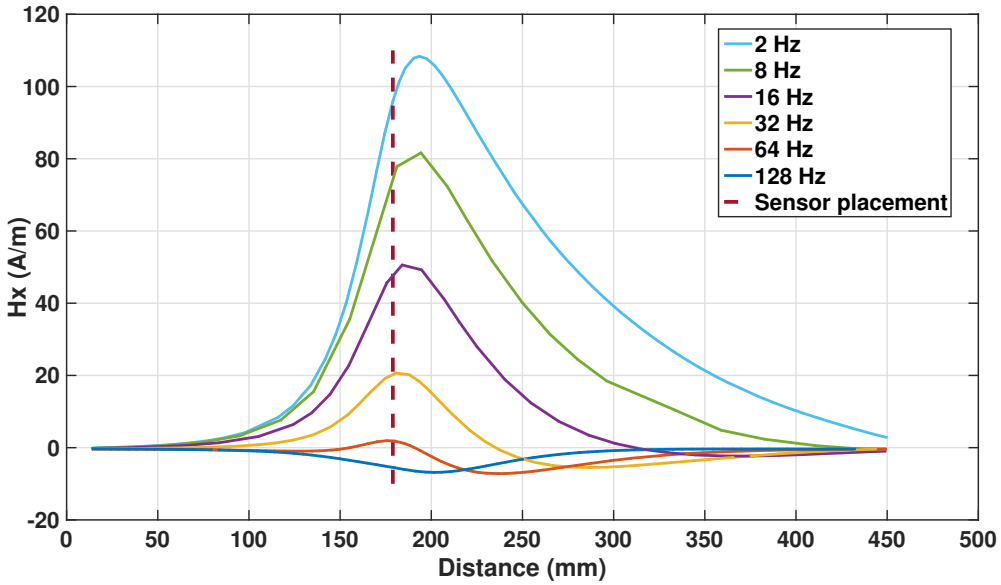

Figure 3.6: The reading of the sensors in positions B as the function of the piston position (measured X component)

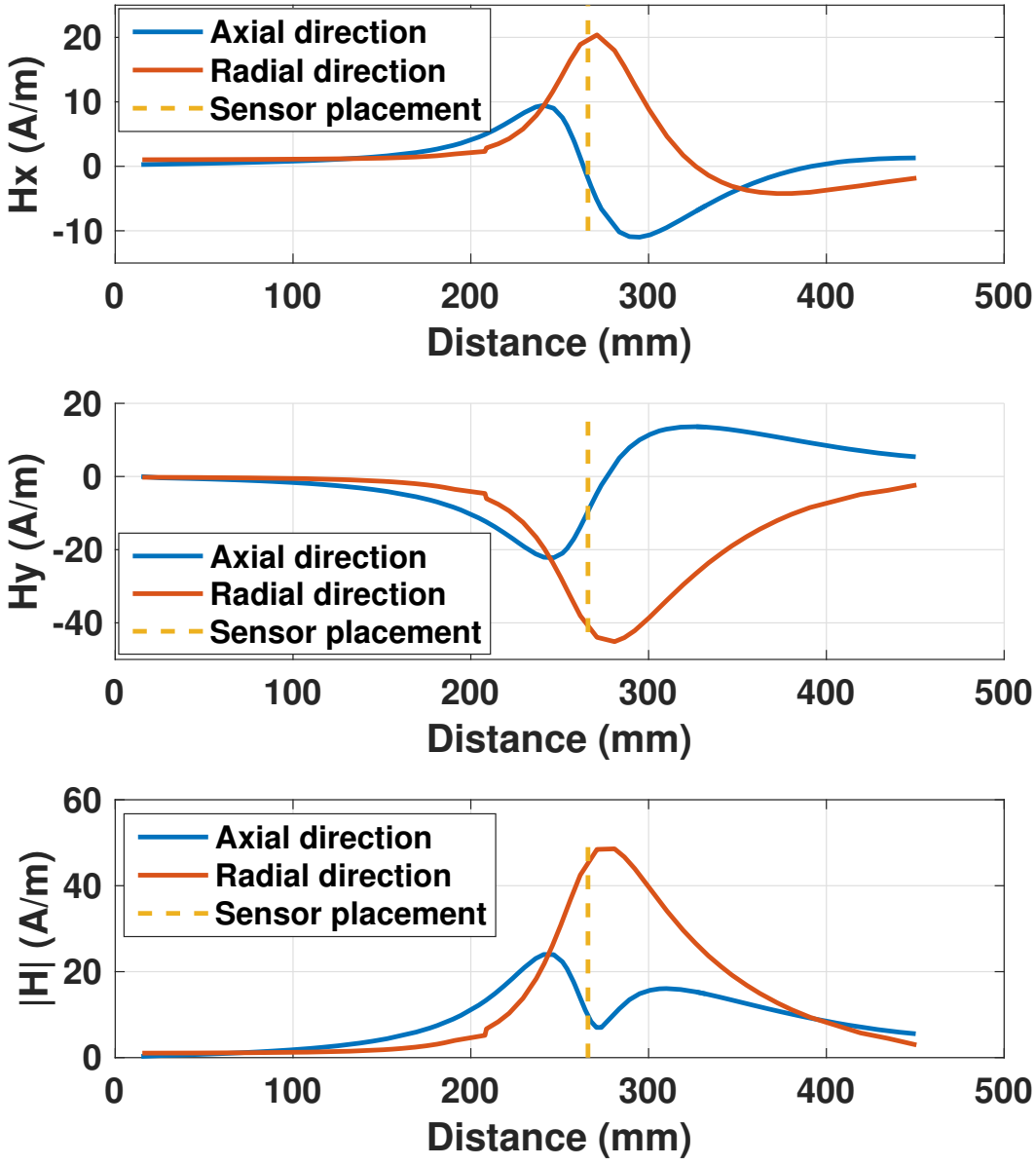

Figure 3.7: Axial and radial field for 32 Hz excitation frequency a) X component (in-phase with current), b) Y component, c) modulus

Chapter 4

Saddle coil sensor

The second method of non-contact detection of the piston rod inside the cylinder is using of two saddle coils that are installed on opposite sides of the cylinder and connected in series so that the magnetic field of both is co-directed. The characteristics of the coils, namely its inductance and resistance at different excitation frequencies are given in Table 4.1. The RMS voltage was $V_{RMS} = 1.886\ V$ and the RMS current flowing through was dependent on the excitation frequency of these saddle coils, for example for $f_{exc} = 50\ Hz$, the RMS current was I=99 mA and for f_{exc} =1 kHz the RMS current was 82 mA. The saddle coils were excited by a waveform generator with an internal resistance of 50 Ω.

	DC	AC 100 Hz	AC 1 kHz
L (mH)	-	10.3979	5.0114
R (Ω)	17.8	20.3537	27.7282

Table 4.1: Parameters of the saddle coils

4.1 FEM simulation

For preliminary results, I made a FEM simulation. The model was simulated for excitation from 4 Hz to 64 Hz and the value of the current flowing through the coil was constant and equal to 90 mA. The properties of the materials are given in Table 4.2. Sensors are at a distance of 2 mm from the surface of the cylinder in the simulation. Axial(Z) component of the magnetic field near the end of the piston is shown in Figure 4.1, and indeed we can see why the graph reaches the maximum value at the end of the piston. The resulting axial component of the magnetic field for different piston position in axial is shown in Figure 4.3. You can see, that the shape of graphs is similar to one we got in simulations with the axial coil. The blue dashed line in the chart is the position of the piston at the time of the passage of the sensor.

The radial component of the magnetic field is shown in Figure 4.2. It can be seen that the body of the piston rod amplifies the radial magnetic component, thanks to this it is also possible to use the measurement of the radial component to detect the piston. The total change of the real component

during the passage of the piston is 15 A/m for f_{exc}=16 Hz. The amplitude of this component is higher since the magnetic field of the saddle coils is co-directed with the radial component of the magnetic field which we measure. In the next chapter, we will give preference to the placement of sensors that measure the axial component of the magnetic field.

The reasons for the decrease in sensitivity with an increase in the excitation frequency are the same: eddy currents in the aluminum tube and eddy currents in the piston rod. We see from the results that their influence up to 16 Hz does not matter much and then it starts to grow.

Material	El. conductivity (MS/m)	μ_r
The iron rod	10.3	1200
The aluminum piston and tube	38	1.000021

Table 4.2: The properties of the materials in the simulation with the saddle coils

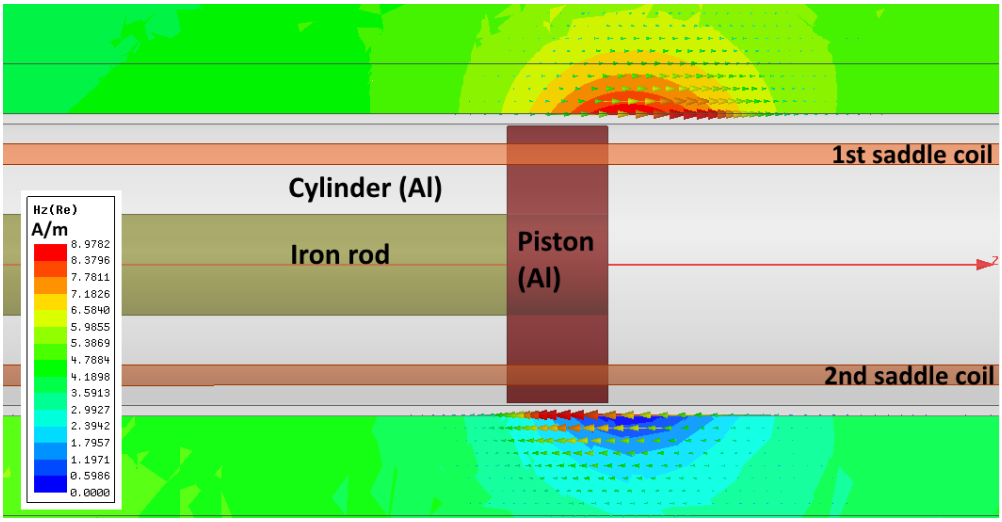

Figure 4.1: FEM Simulation - Axial field for 4 Hz excitation frequency

4.2 Measurement

As in the case of axial excitation, five sensors were placed on the surface of the cylinder using the sensor holders with a distance between them of 9 cm to measure the magnetic field along the whole tube. For this installation, we used ready-made evaluating modules DRV425EVM, and the connection scheme was the same as in Figure 2.6. The results of the measurement are shown in Figure 4.6. The irregularities with a 64 Hz plot are caused by eddy currents. To confirm that this roughnesses are caused by eddy currents, we measured the position with the plastic piston instead of aluminum, results of the measurement are shown in Figure 4.7. It really shows that the graph with the plastic piston has a smooth shape in contradistinction to the aluminum piston.

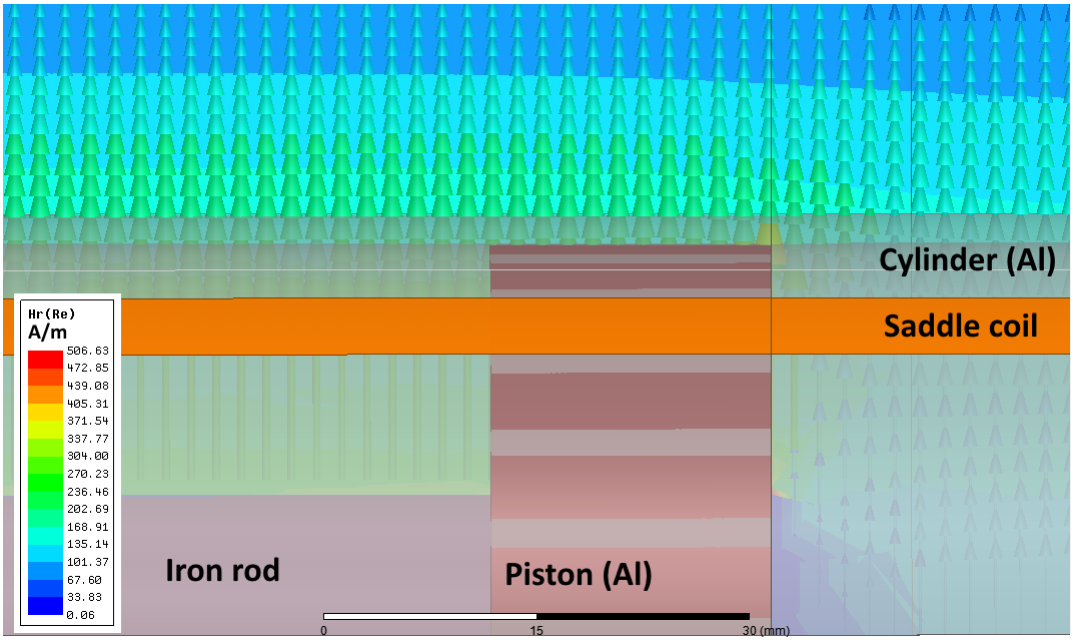

Figure 4.2: FEM Simulation - Radial field for 4 Hz excitation frequency

At low frequencies, the permeability of the piston rod is more important, than eddy currents. The results of the simulation and the result of measurements perfectly fit. As in the case of the saddle coils and the case of axial excitation, we must find a compromise in the choice of the operating excitation frequency. If the piston moves quickly we should choose a higher frequency at the expense of signal strength.

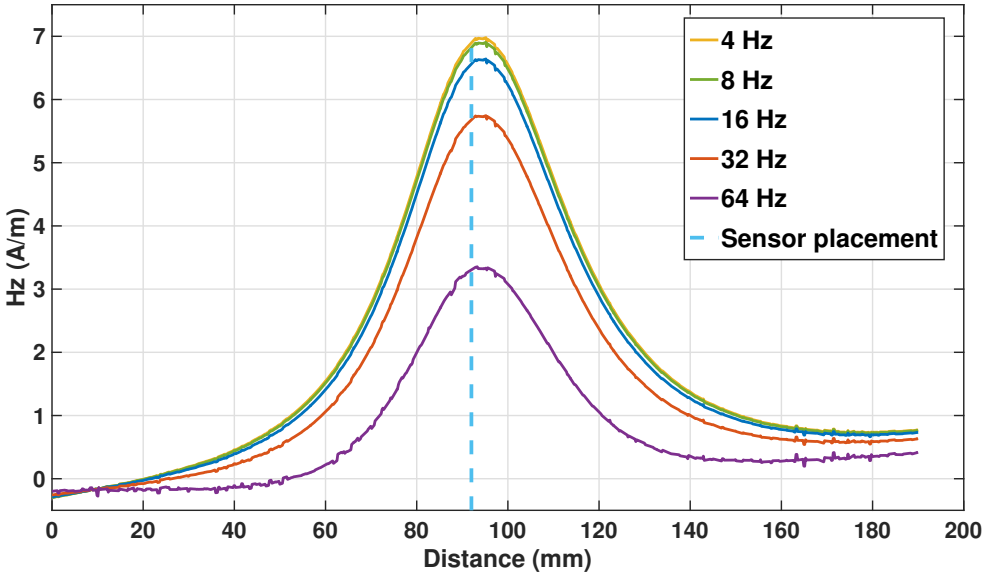

Figure 4.3: Axial field Hz - FEM simulation for f= 4 Hz to 64 Hz (real part)

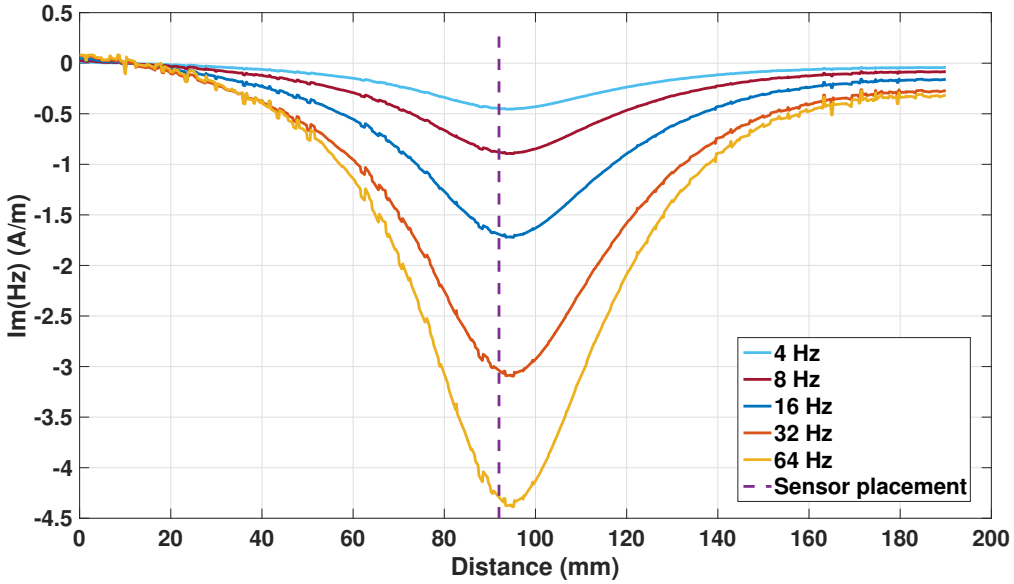

Figure 4.4: Axial field Hz - FEM simulation for f= 4 Hz to 64 Hz (imaginary part)

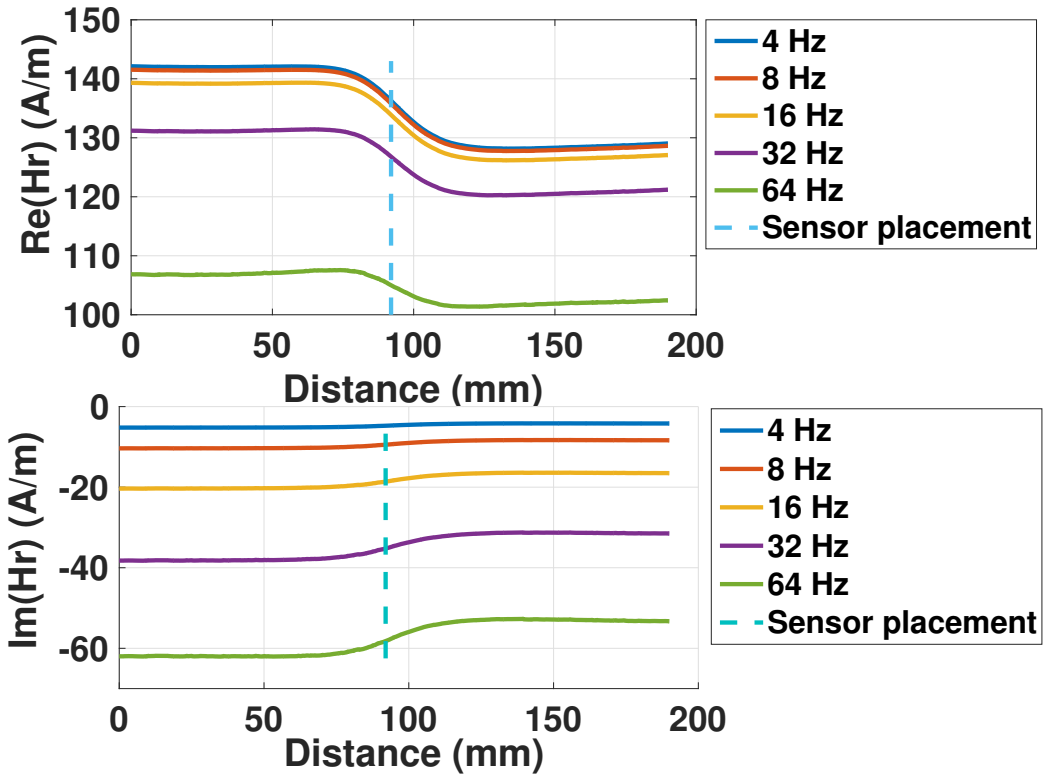

Figure 4.5: Radial field Hr - FEM simulation for f= 4 Hz to 64 Hz a) real component b) imaginary component

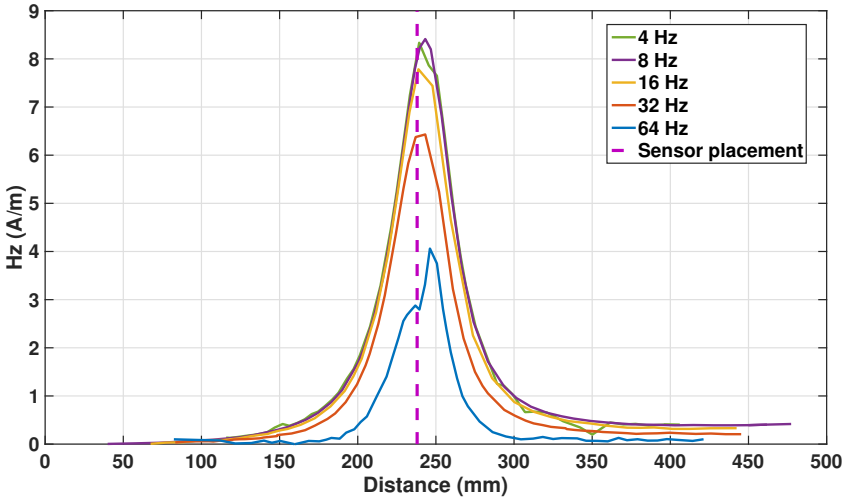

Figure 4.6: Axial field Hz - measurement (real part) for f= 4 Hz to 64 Hz

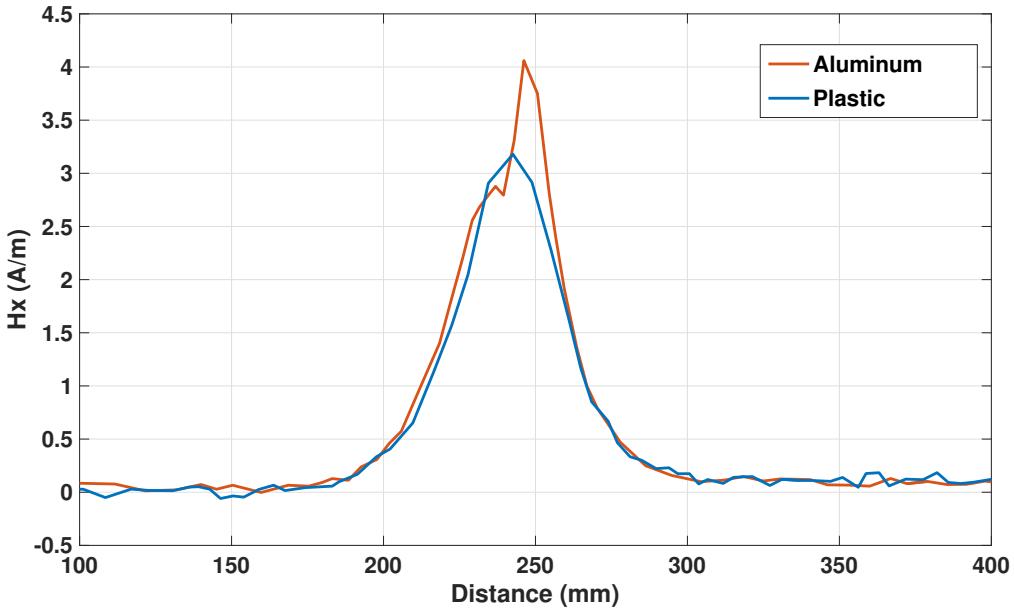

Figure 4.7: Axial field - Measuring the position of the piston made of two different materials at 64 Hz

Chapter 5

Design of the multi-sensor transducer with saddle coils

Based on previous measurements and simulations for both the solenoid and the saddle coils, we selected the saddle coils. The sensors were positioned parallel to the cylinder so that the sensors measured Z-component of the magnetic field since the main reason for this is that such a placement of the sensors is easy and makes the whole sensor small so that it would find more use in the industry.

Reasons for this:

1. Easier to install on the existing cylinders. It is enough just to attach the saddle coils to the surface of the cylinder and insert a PCB board with the sensors inside one of them

2. the signal from the sensors is strong enough

We designed a PCB board with 16 fluxgate sensors so that the distance between the sensors was 3 centimeters and they were evenly distributed throughout the cylinder. The sensor connection was taken from the datasheet and it was described in detail in the Subsection 2.4.1. How the PCB board looks like is shown in Figure 5.1 and experimental model at the laboratory is shown in Figure 5.2. Dimensions of the PCB board are such that it has a width of 33 mm and a length of 483 mm, and this was chosen in order to fit inside the saddle coil ideally. PCB board is double sided (two copper layers).

5.1 Electrical connection of the 16 sensors

In Figure 5.3 it is shown how we connected all 16 sensors. The output voltage and the reference signal of each sensor goes to a flat bus that is connected to a multifunctional DAQ device, namely, NI USB-6212. Unfortunately, this card has only 16 analog inputs, so we did not use the reference signal of each sensor, and as the reference, we used the GND. The only change that we made in the electrical connection of every sensor, which is shown in Figure 2.6, is that the pins of the RSEL0 and RSEL1 now are connected to the GND. This means that we switched the default settings of ratio-metric reference equal to VDD/2

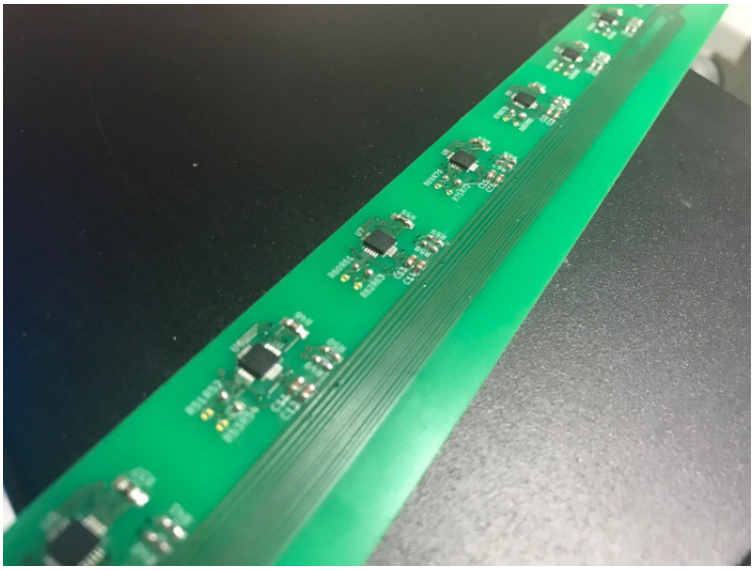

Figure 5.1: PCB board with 16 fluxgate sensors

to the fixed reference of 2.5 V, this was done to improve the stability of the output signal. The rest of the electrical connection including the voltage regulator, the diode, the capacitors are similar to what was described in the chapters with the axial coil and the saddle coils. Each block in the electrical circuit is a hierarchical sheet that includes the connection of the sensor, and this is done for clarity. The bill of the materials that was used for the PCB board is listed in Table 5.1.

DESIGNATORS	DESCRIPTION
D1	LED, Green, 120°,450 mcd at 20 mA, 0805
D2	Diode, 600 V/1 A, DO41, Uf= 1.2V, trr= 200 ns
U1,U2, ... U16	Fluxgate sensor DRV425
U17	7805 5V Voltage Regulator, TO-220
R2	RES, 1 k, +/- 1%, 0.1 W, 0603
C33,C34	CAP, CERM, 1 uF, 25 V, +/- 10%, X7R, 0603
P1	Header, 100 mil, 17x2, Copper, Straight, TH

Table 5.1: Bill of materials for connection with 16 sensors

5.2 Program

We wrote a program in the Lab View that contains a software (digital) Lock-In amplifier for all 16 sensors on our PCB board and is able to receive and process their output signal. How this program looks like in Figure 5.4.

From sensor's output signal we can extract the real and imaginary component as well as the phase. The number of samples for the triggering is set for one period of the reference signal, which is taken from the generator and is

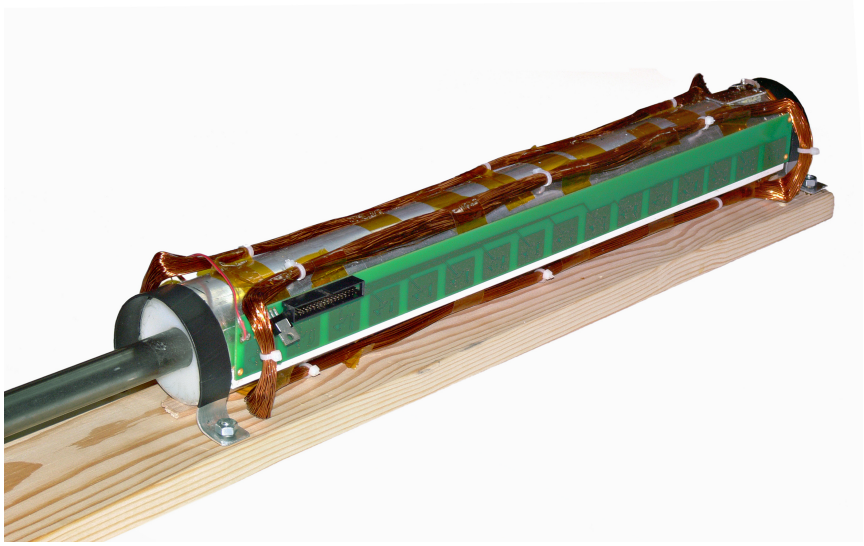

Figure 5.2: Experimental model at the laboratory with the PCB board [19]

calculated by Equation 5.1. The value of the Sample Rate was set to 25000 samples per channel per second i.e. for the exciting frequency of 32 Hz, the Number of Samples was approximately 780.

$$Number\ Of\ Samples = \frac{Sample\ Rate}{Frequency\ of\ Generator} \tag{5.1}$$

Schematic diagram of the program is shown in Figure 5.5. As described above for the transfer from analog to digital form of the signals from the sensors we used a multifunctional I/O device NI USB-6212. Signals from the sensors were digitally multiplied with the reference signal without a phase shift (the result is the X component or real part) and with a phase shift of 90 degrees (the result is the Y component or imaginary part). For filtering the resulting real part and the imaginary part, we used two filters. The first one is Mean, which returns the average value of the input signal, and the second one is Butterworth. The low cut-off frequency of the Butterworth filter is set at 0.5 Hz. After this, the signals are processed using three methods described in Section 5.3.

This program also contains the processing of the output signal from the reference position potentiometric sensor, which is connected to the multimeter and used to obtain the maximum achievable resolution for our position sensor. To convert the voltage on the sensor to distance, we used Equation 5.2.

$$l(mm) = \frac{V_{out}(mV)}{8(\frac{mV}{mm})} \tag{5.2}$$

Then we compared the results of measurements from our sensors to the reference position sensor along the entire length of the cylinder. Our program also displays in real time voltage on the sensors, how it changes with a passage of the iron rod, and there is the possibility of writing data to the file, the

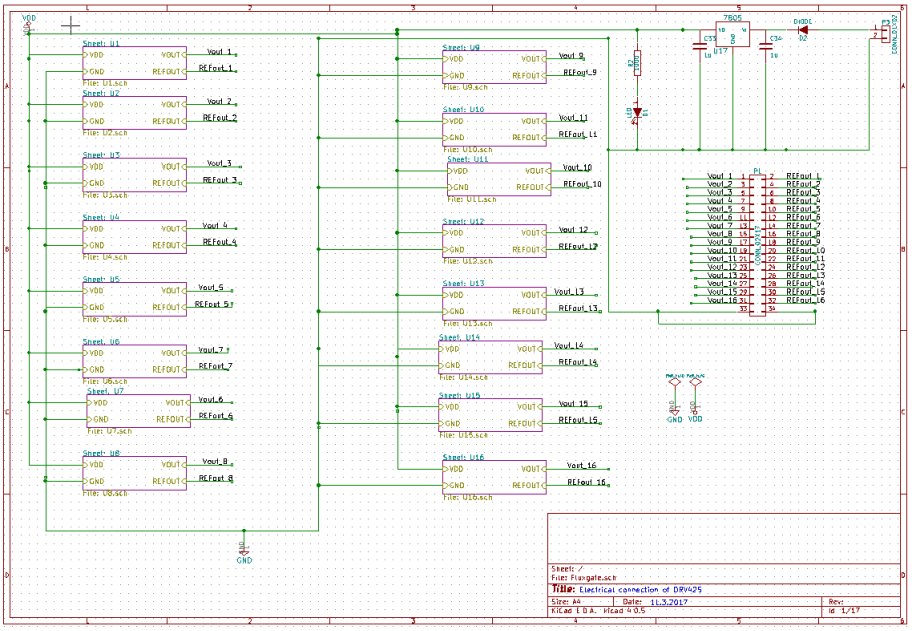

Figure 5.3: Electrical connection of the 16 sensors

ability to calibrate the sensor and adjust the offsets. It is recommended to set the offset to 0 before starting the measurement (when the piston is completely pushed out of the cylinder).

5.2.1 User manual for the program in LabView

There will be described some steps which you must follow to correctly make a measurement of the position of the piston rod in the pneumatic cylinder.

1. Select the input channels and device where the sensors will be connected, Max and Min voltage and Terminal Configuration in the "Chanel settings" block.

2. Select the "Digital Ref" tab in the "Trigger settings" block and set Digital Ref Trigger Source to your generator from which the reference is taken. You can also set the low cut-off frequency for Butterworth filter in this block.

3. Connect the multimeter to obtain the output voltage from the reference sensor in "Agilent 34401A" block and set the Exciting frequency of generator in "Timing settings" block.

4. Configure the log file in "Log settings" block.

5. Run the program, take the piston out then press the Null key. Now our sensors are without offset value and it is possible to measure the position of the piston inside the cylinder. For better performance of our invented methods, it is recommended to calibrate the sensor. Set the piston rod in

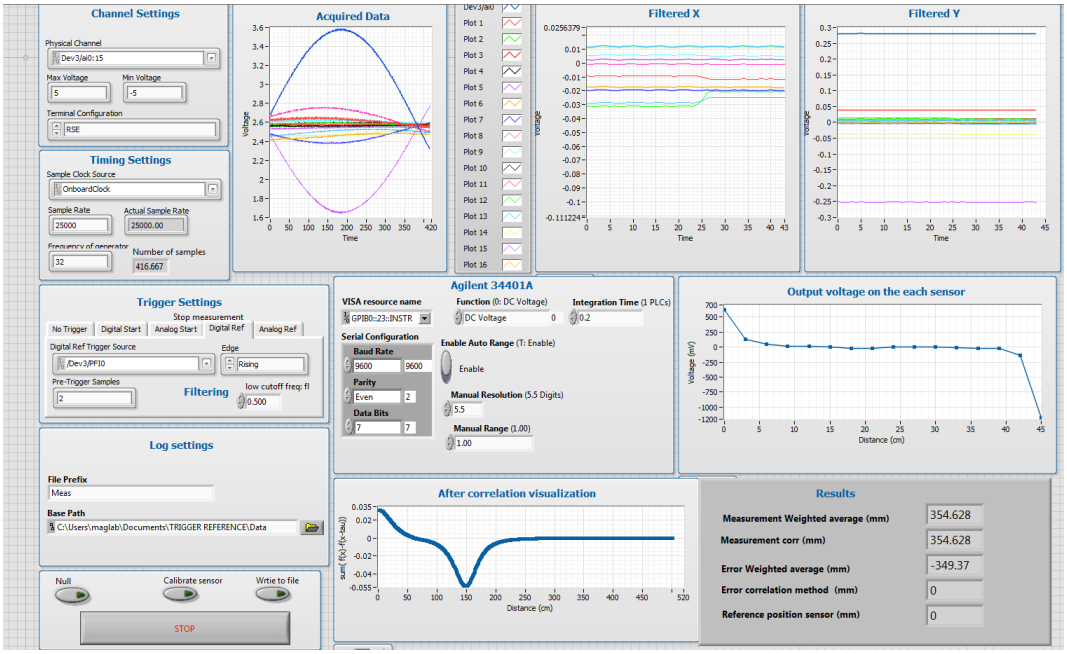

Figure 5.4: Front panels in our LabView program

such a position that the output voltage on one of the sensors is maximum and press the "Calibrate sensor" key.

6. The calculation position of the piston is displayed in the "Results" block. At the end of the measurement, stop the program with the "Stop" key.

   The voltage on all sensors in real time can be seen on the graph "Output voltage on the each sensor". You can also see the acquired date, filtered X and Y component on the corresponding graphs.

5.2.2 Lock-In Amplifier

Lock-in amplifiers are used to detect and measure very small AC signals - all the way down to a few nanovolts. Accurate measurements can be made even when the small signal is obscured by noise sources many thousands of times larger. Lock-in amplifiers use a technique known as phase-sensitive detection to extract the component of the signal at a specific reference frequency and phase. Noise signals, at frequencies other than the reference frequency, are rejected and do not affect the measurement [20] Lock-in measurements require a frequency reference. Typically, an experiment is excited at a fixed frequency (from an oscillator or function generator), and the lock-in detects the response from the experiment at the reference frequency. In the following diagram, the reference signal is a square wave at frequency ω_r. This might be the sync output from a function generator. If the sine output from the function generator is used to excite the experiment, the response might be the signal waveform shown below. The signal is $V_{sig}\sin(\omega_r t + \theta_{sig})$ where V_{sig} is the

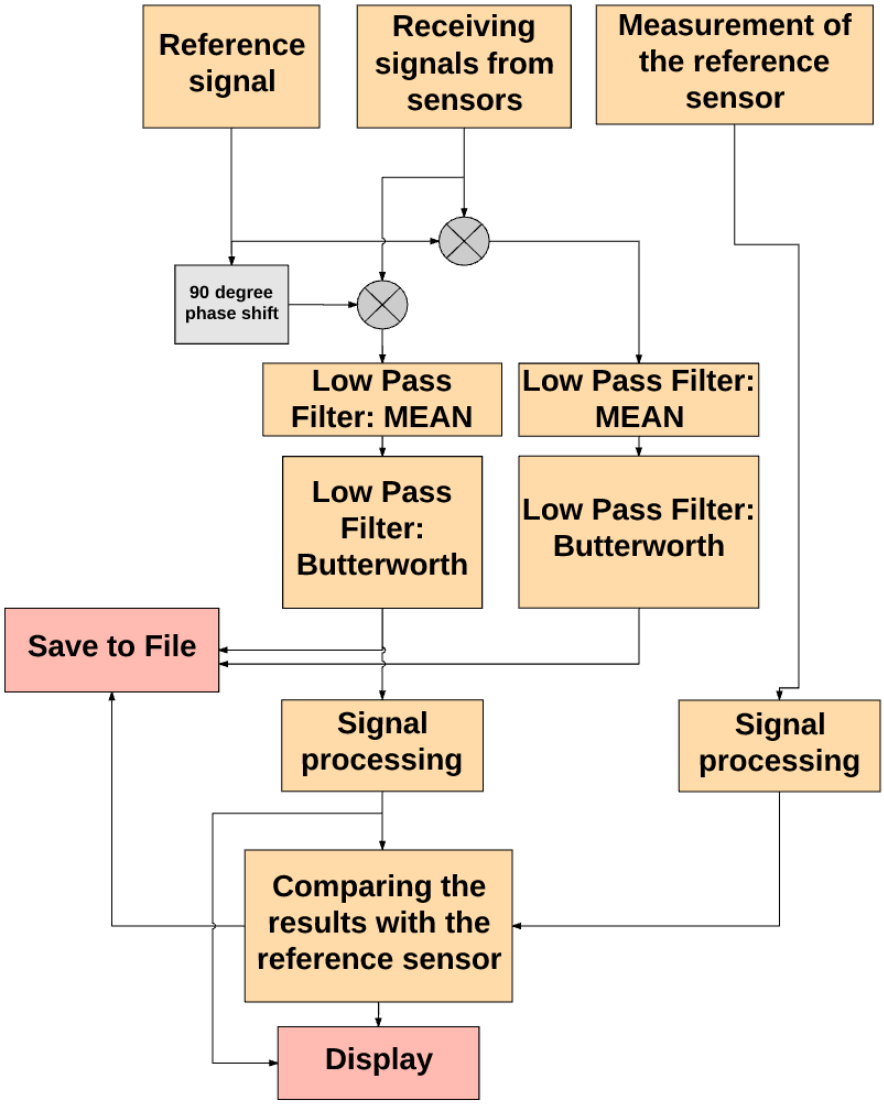

Figure 5.5: Schematic diagram of the program

signal amplitude, ω_r is the signal frequency, and θ_{sig} is the signal's phase. Lock-in amplifiers generate their own internal reference signal usually by a phase-locked-loop locked to the external reference. The internal reference is $V_L \sin(\omega_L t + \theta_{ref})$

5.2.3 Mathematical background of SD

The measured and the reference signals are described in Equation 5.3. [20]:

$$\begin{aligned} V_{sig} \sin(\omega_r t + \theta_{sig}) \\ V_L \sin(\omega_L t + \theta_{ref}) \end{aligned} \tag{5.3}$$

Then signal after mixer (multiplier) is:

$$\begin{aligned} V_{psd} = V_{sig}V_L \sin(\omega_r t + \theta_{sig}) \sin(\omega_L t + \theta_{ref}) = \\ \frac{1}{2}V_{sig}V_L \cos([\omega_r - \omega_L]t + \theta_{sig} - \theta_{ref}) - \\ \frac{1}{2}V_{sig}V_L \cos([\omega_r + \omega_L]t + \theta_{sig} + \theta_{ref}) \end{aligned} \tag{5.4}$$

The PSD output consists of two AC signals, one at the difference frequency (ω_r - ω_L) and the other at the sum frequency (ω_r + ω_L).

If the PSD output is passed through a low pass filter with cut-off frequency below $f_r + f_L$, the latter signal component will be suppressed. However, if ω_{sig} equals ω_{ref}, the difference frequency component will be a DC signal. In this case, the filtered PSD output will be:

$$V_{psd} = \frac{1}{2}V_{sig}V_L \cos(\theta_{sig} - \theta_{ref}) \tag{5.5}$$

This is a very nice signal - it is a DC signal proportional to the signal amplitude. A lock-in with a single PSD is called a single-phase lock-in and its output is $V_{sig}cos(\theta)$, where $\theta = (\theta_{sig} - \theta_{ref})$.This phase dependency can be eliminated by adding a second PSD. If the second PSD multiplies the signal with the reference oscillator shifted by 90,° i.e. $V_L \sin(\omega_L t + \theta_{ref} + 90°)$,its low pass filtered output will be:

$$V_{psd} = \frac{1}{2}V_{sig}V_L \sin(\theta_{sig} - \theta_{ref}) \tag{5.6}$$

Now we have two outputs: one proportional to $\cos\theta$ and the other proportional to $\sin\theta$. We call the first output X (from Equation 5.5) and the second Y (from Equation 5.6). These two quantities represent the signal as a vector relative to the lock-in reference oscillator. X is called the 'in-phase' (or real) component and Y the 'quadrature' (or imaginary) component. By computing the magnitude (R) of the signal vector, the phase dependency is removed.

$$R = \sqrt{X^2 + Y^2} = V_{sig} \tag{5.7}$$

R measures the signal amplitude and does not depend upon the phase between the signal and lock-in reference.A dual-phase lock-in has two PSDs with reference oscillators 90° apart, and can measure X, Y and R directly. In addition, the phase (θ) between the signal and lock-in is defined as:

$$\theta = arctan(Y, X) \tag{5.8}$$

5.3 Signal processing

For the processing signals from the sensors, we used three methods. One of them is the calculation of the piston rod position using the arithmetic average weighted. For this approach, only three sensors for calculating are used, one that has the highest output voltage, and the other two on both sides of it.

Equation 5.9 for calculating weighted average:

$$Position = \frac{V_{max-1} \cdot n_{max-1} + V_{max} \cdot n_{max} + V_{max+1} \cdot n_{max+1}}{V_{max-1} + V_{max} + V_{max+1}} \tag{5.9}$$

where

V_{max} - the maximum output voltage on the sensor
n_{max} - the number of the sensor
V_{max-1} - the voltage on the sensor on one side
V_{max+1} - the voltage on the sensor on the other side
n_{max-1} - the number of the sensor on one side
n_{max+1} - the number of the sensor on the other side

The second method operates with all outputs of the sensors simultaneously and uses the concept of least squares fitting.[22] For this method, the signal that was approximated using Curve Fitting Tool in Matlab was obtained from the measurement at 32 Hz. This approximation is shown in Figure 5.6 and was made by Ing. Jan Vyhnánek.

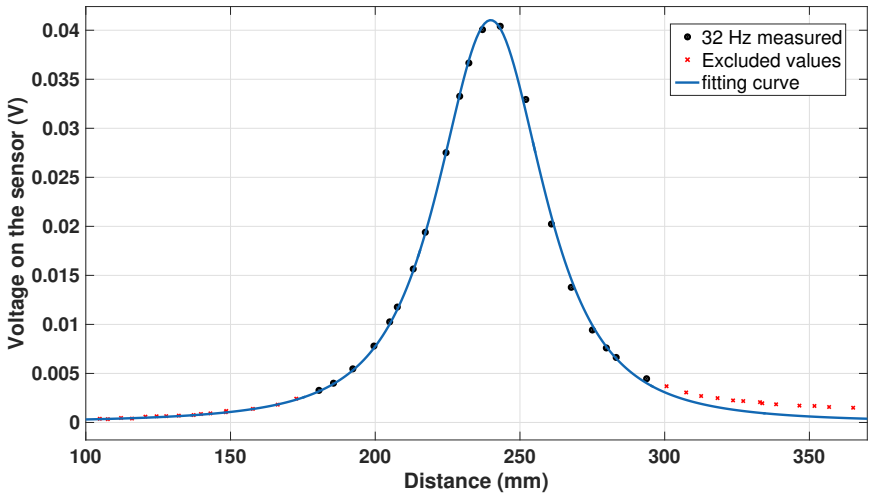

Figure 5.6: Fitting curve of measured data at 32 Hz

The equation of this approximation function:

$$f'_{aproximated} = \frac{900.5}{((x-\tau)^2 + 783.9)^{\frac{3}{2}}} \tag{5.10}$$

where τ is the value that indicates the position of the piston rod.

Based on this equation it can be asserted, that our piston is monopole. In fact, this is a dipole, but the second end of the piston rod is very far away, and we can regard it as a monopole. For calculating the position of the piston, we used least-squares fitting method.

Optimum criterion :

$$\min_{x \in N} \sum (f(x) - f'(x-\tau))^2 \tag{5.11}$$

We want to find the smallest value for all values obtained; this minimum will indicate where the piston rod is located.

And finally, the third method is a small improvement of the second. This is normalization, for each sensor by measuring we found its maximum output voltage when passing iron rod. And then the value of which is allowed to be processed is divided by the maximum value for each sensor, in this way we get a signal in the range from 0 to 1. The following steps are the same as in method with least square fitting. We want to calculate the minimum difference between the approximated function and the function that we get from the output signals of the sensors.

The results of these three methods will be presented in Chapter 6.

Chapter 6

Results

The results of our three methods at 32 Hz are shown in Figure 6.1. As described above, our reference sensor was a potentiometric linear transducer with linearity $\pm\%0.05$. Based on this picture, we can conclude that based on simple calculation methods such as weighted average arithmetic, a position error of 5 mm is possible. Another more advanced method, such as calculating the optimum function, requires more computational resources but allows you to achieve the error of 2 mm. The standardized method did not give much improvement in reducing error. Of course, with a more dense placement of sensors and finding more optimal methods for calculating the position of the piston, one can achieve even better resolution. It can clearly be seen that the outputs from the sensors are the same in different places of the pneumatic cylinders, this is shown in Figure 6.2 and 6.3 for 2 different methods: axial coil sensor and saddle coil sensor. The results for the axial coil sensor were presented at Intermag conference 2017 in Dublin, Ireland. The saddle coils results were submitted to the Eurosensors conference and the paper with Axial coil sensor [18] was submitted for publication in IEEE Transactions on Magnetics.

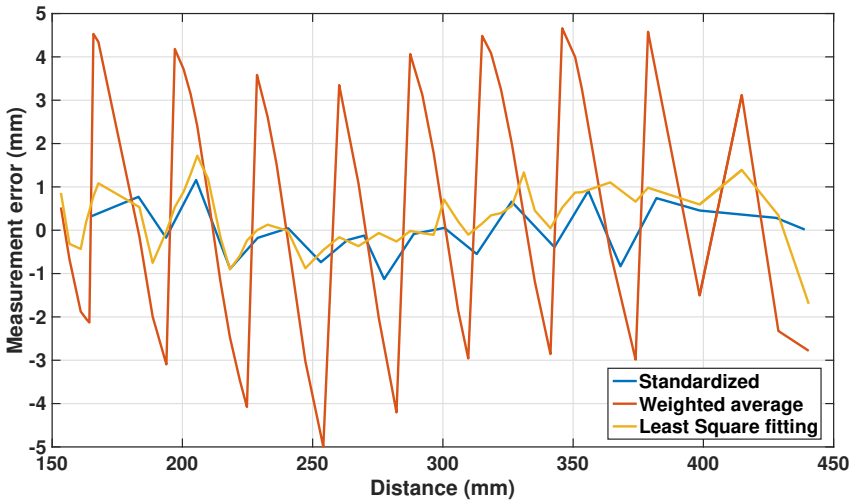

Figure 6.1: Measurement error as the function of the piston position

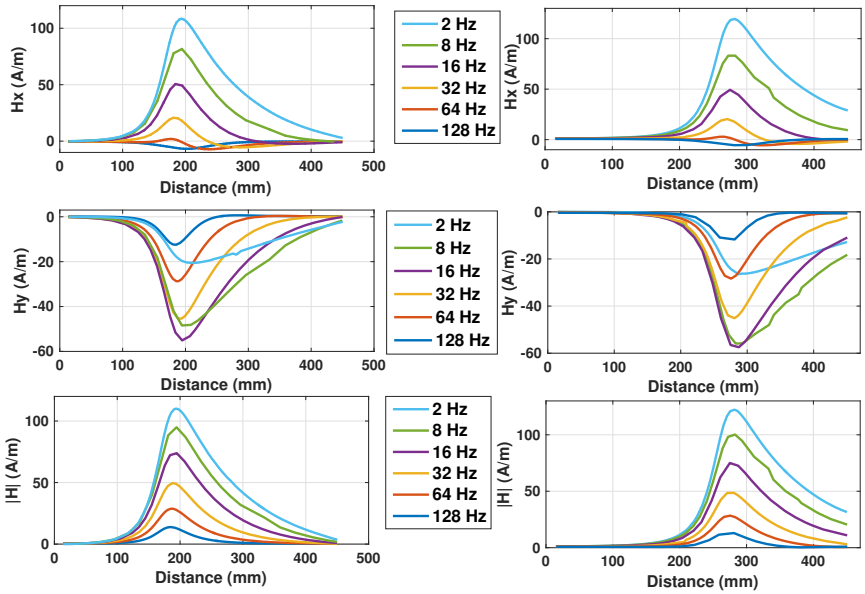

Figure 6.2: Axial coil sensor - The measured axial component of the magnetic field using two different sensors a) real part b) imaginary part c) modulus

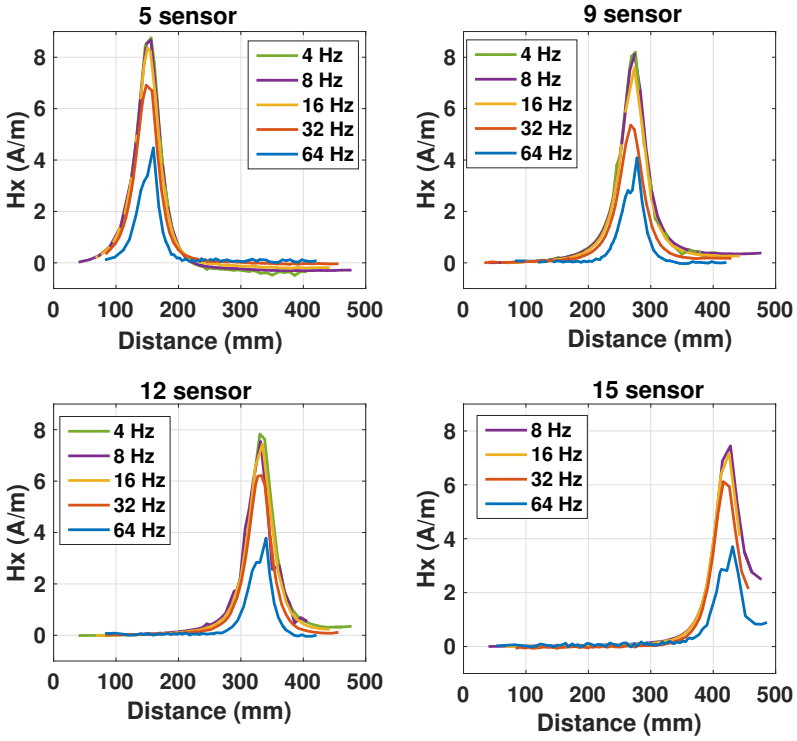

Figure 6.3: Saddle coil sensor - The measured real part of the axial component of the magnetic field using four different sensors

Chapter 7

Conclusion

In this thesis I have shown that the position of the piston in the pneumatic cylinder can be measured by AC magnetic method without the permanent magnet. The sensor parameters were optimized by the FEM simulation and accuracy was verified by potentiometric reference position sensor.

Using axial field excitation and an array of radially oriented fluxgate sensors on the cylinder surface or using the saddle coils with the sensors, which measure axial component of the magnetic field an accuracy of 1 mm and resolution of 0.1 mm is achievable. The sensor linear range is 4 cm. For longer strokes, linear array of sensors spaced 2 to 3 cm should be used. The main advantages of the new method are [18]:

1. it can be used on existing cylinders, both the coil and sensors are mounted outside the cylinder.
2. no need for expensive non-magnetic stainless steel piston rod.
3. resistance to the rod geometrical and magnetic imperfections, rotation (verified by measurement with several rods, some of them with a curvature and some of them exposed to mechanical shocks.
4. low price

The disadvantage of these methods is that the excitation frequency should be kept low, so that the magnetic field penetrates into the cylinder, and this limits the dynamic response of the transducer. It needs to find a compromise between the exciting frequency and the signal strength. One of them fundamental factors that affects this choice is the speed of the piston movement. But one main rule: the higher the speed of the piston rod, the higher the exciting frequency.

We still have to solve temperature problem, because our method is based on permeability of the soft iron rod. And it is well known that permeability is dependent on the temperature of the material.

Bibliography

[1] Sheila Campbell, Norgren Inc.: *Guidelines for Selecting Pneumatic Cylinders*, Machine Design, September 2011

[2] Kamarton: *3D animated pneumatic cylinder (CAD)*, Wikipedia, March 2008

[3] Majumdar, S.R. (1995): *Pneumatic System: Principles and Maintenance.* New Delhi: Tata McGraw-Hill.

[4] The Engineering Toolbox: *Pneumatic air cylinders - air pressure and force exerted calculator*, Pneumatic Cylinders - Force Exerted at `http://engineeringtoolbox.com/pneumatic-cylinder-force-d_1273.html`

[5] I. Herceg: *Taking a Position on Hydraulic Cylinder Sensors, Hydraulics & Pneumatics.* July 2015, 24-27.

[6] Sorin Fericean, Andrea Hiller-Brod, Albert Daniel Dorneich, Markus Fritton: *Microwave Displacement Sensor for Hydraulic Devices".* Microwave Displacement Sensor for Hydraulic Devices", IEEE Sensors Journal, Vol. 13, No. 12, December 2013

[7] L. Shih-Yuan, L. Jyun and S. S. Lee: *"The study of the piston driving and position sensing for a linearly moving piston pump,".* Automatic Control Conference (CACS), 2014 CACS International, Kaohsiung, 2014, pp. 287-291

[8] K. Suzumori, J. Tanaka and T. Kanda: *Development of an intelligent pneumatic cylinder and its application to pneumatic servo mechanism,.* Proceedings, 2005 IEEE/ASME International Conference on Advanced Intelligent Mechatronics., Monterey, CA, 2005, pp. 479-484

[9] A. A. M. Faudzi, K. Suzumori and S. Wakimoto: *"Design and control of new intelligent pneumatic cylinder for intelligent chair tool application,".* Proceedings, 2009 IEEE/ASME International Conference on Advanced Intelligent Mechatronics, Singapore, 2009, pp. 1909-1914

[10] Soon Yong Yang, Min Cheol Lee, Man Hyung Lee and S. Arimoto, *Measuring system for development of stroke-sensing cylinder for automatic*

excavator, in IEEE Transactions on Industrial Electronics, vol. 45, no. 3, pp. 376-384, Jun 1998.

[11] Stransky a Petrzik company, Pneumaticke valce spol. s.r.o. at `https://www.stranskyapetrzik.cz/en/`

[12] DRV425 Fluxgate Magnetic-Field Sensor, Texas Instruments datasheet at `http://www.ti.com/product/DRV425/datasheet`

[13] Wikipedia contributors: *"Penetration depth"*, Wikipedia, The Free Encyclopedia, `https://en.wikipedia.org/wiki/Penetration_depth`

[14] P. Ripka: *Magnetic Sensors and Magnetometers*, Artech House Publish, ers. ISBN-10: 1580530575, p.75

[15] P. Ripka, Michal Janosek, Mattia Butta, William S. Billingsley, Eva M. Wakefield: *Crossfield effect in commercial fluxgate and AMR sensors*, Journal of ELECTRICAL ENGINEERING, VOL 61. NO 7/s, 2010, 13-16

[16] P. Ripka, J. Vyhnánek, A. Chirstov: *Crossfield response of industrial magnetic sensors*, subm. to Journal of Applied Electromagnetics and Mechanics (IJAEM)

[17] Wikipedia contributors: *"Finite element method"*, Wikipedia, The Free Encyclopedia, `https://en.wikipedia.org/wiki/Finite_element_method`

[18] P. Ripka, A. Chirtsov, V. Grim: *Contactless Piston Position Transducer with Axial Excitation*, proc. Intermag 2017., subm. to IEEE Trans. Magn.

[19] J. Vyhnanek, P. Ripka, A. Chirtsov: *Linear position sensing through conductive wall without permanent magnet* , subm. to proc. Eurosensors, 2017

[20] Stanford Research Systems: *About Lock-In Amplifiers*, Application Note #3, `http://thinksrs.com/downloads/PDFs/ApplicationNotes/AboutLIAs.pdf`

[21] Electronics Hub, *Understanding 7805 IC Voltage Regulator*, SEPTEMBER 5, 2015 at `http://electronicshub.org/understanding-7805-ic-voltage-regulator/`

[22] Mathworks Curve Fitting Toolbox: *Least-Squares Fitting* at `https://mathworks.com/help/curvefit/least-squares-fitting.html`

Appendix A

Contents on the CD:

1. This bachelor thesis in PDF
2. Program in LabView and measured data. The program is accompanied with a user manual: Readme.txt
3. J. Vyhnanek, P. Ripka, A. Chirtsov: *Linear position sensing through conductive wall without permanent magnet*
4. P. Ripka, A. Chirtsov, V. Grim: *Contactless Piston Position Transducer with Axial Excitation*
5. P. Ripka, J. Vyhnánek, A. Chirstov: *Crossfield response of industrial magnetic sensors*

Appendix A

Contactless Piston Position Transducer with Axial Excitation

Pavel Ripka, Andrey Chirtsov, and Vaclav Grim

Czech Technical University, Faculty of Electrical Engineering
Prague, Czech Republic

Existing piston position sensors require either drilling precise hole into the piston bar or mounting permanent magnets or measuring device inside the pressurized cylinder. We present a new solution for aluminum pneumatic cylinders, which uses the ferromagnetic bar inside the solenoid as a marker and linear array of fluxgate sensors as a scale. Instead of relying on DC remanence we use active AC excitation; the reading is resistant against external fields, both DC and AC. Using sensor array allows to compensate for temperature effects. The linear stroke of the individual sensor is 40 mm, so that array density should be about 30 mm. 1 mm position resolution is achievable. The weak point of the new transducer is the response time: for fast moving pistons the excitation frequency should be high, which leads to weaker signal and lower resolution.

***Index Terms*—About four key words or phrases in alphabetical order, separated by commas.**

I. Introduction

Piston position Transducers for hydraulic and pneumatic cylinders are more demanded by industry, as they are necessary for fine control.

Position sensor for hydraulic cylinders are usually in a shape of a long probe which is inserted into the deep narrow blind hole in the cylinder rod [1]. Non-contact sensors based on magnetostrictive principle (using toroidal permanent magnet in the piston) or variable inductance replace potentiometer sensors, which are cheap but have limited lifetime due to friction. The disadvantage of this type of sensors are the cost and reliability issues associated with the necessity of the long "gun drilled" hole in the rod and necessary fitting for the sensor, which resides inside the cylinder. Similar disadvantages exist for the microwave position sensors [2]. Vision-based sensors [3] and incremental optical piston position sensors [4, 5] were also developed, but they did not found industrial applications due to the reliability issues. Some systems use magnetic scale of a piston rod together with Hall sensors [6].

External monitoring of the hydraulic piston position is a challenge, as the walls of hydraulic cylinders are usually made of carbon steel which is ferromagnetic. The field of permanent magnet embedded in the piston is therefore shielded by the ferromagnetic barrel wall and distorted by both the wall and rod. Precision better than 5 mm is therefore hardly achievable. Some special hydraulic cylinders such as those used in water hydraulic systems have composite shell. For these cylinders inductive displacement sensor can be built using a coil winding in the shell of the cylinder [7].

Pneumatic cylinders usually have aluminum wall which is transparent for permanent magnet and therefore ideal for external sensors. Thanks to the simplicity and non-contact non-invasive capability these sensors are reliable and cost effective. The sensors being used for this application are mainly Hall and AMR, rarely GMR.

However, permanent-magnet based piston position sensors have several disadvantages:

1. They are influenced by external magnetic fields including those induced by DC currents
2. They require non-magnetic stainless steel piston rod, which is expensive. Aluminum cannot be used for this part because of strength requirements
3. Sensor cannot be mounted on existing cylinders if they are not equipped by magnet. Usually the complete cylinder should be exchanged, which is difficult and expensive especially in the case of large machinery.

The distance between the permanent magnet and sensors is nonlinear function of the measured magnetic field. If the ferromagnetic objects are present in the close vicinity, the mentioned function is very complex. Non-linear observer methods has been employed to accurately estimate the piston position in real time [8].

External DC magnetic sensors has been used also for the measurement of a piston position inside the cylinder of free piston engine [9]. The disadvantage of such DC systems without permanent magnet is that they rely on the remanence of ferromagnetic parts which may easily change with time and temperature.

In this paper we introduce novel eddy-current external position sensor for pneumatic cylinders. It uses AC magnetic field excitation and detection by integrated fluxgate sensors.

II. New Sensor Design

In this paper we suggest new AC piston position transducer using axial coil directly wound on the cylinder surface as a field source. The 2 or 3 mm thick electrically conducting cylinder wall has large attenuation, however we show that at low frequencies the field inside the cylinder is still strong

Manuscript received April 1, 2015; revised May 15, 2015 and June 1, 2015; accepted July 1, 2015. Date of publication July 10, 2015; date of current version July 31, 2015. Corresponding author: F. A. Author (e-mail: f.author@nist.gov. Color versions of one or more of the figures in this paper are available online at http://ieeexplore.ieee.org.

Digital Object Identifier (inserted by IEEE).

enough so that the cylinder movement can be observed by external fluxgate sensor.

For the verification of this principle we built a physical model of the pneumatic cylinder using 60 mm diameter barrel pipe made of 2 mm thick aluminum, 10 mm thick aluminum piston and 20 mm diameter steel piston rod. On top of the cylinder we wound single-layer axial coil with parameters in Tab 1.

TABLE 1 HERE

The coil was supplied from the function generator with 50 Ω internal resistance, so that the rms excitation current of 90 mA at low frequencies was decreasing with frequency to 70 mA at 100 Hz. The maximum generated field in the center of the cylinder was 156 A/m at 10 Hz and it was reduced mainly by the shielding effect of the aluminum cylinder to one half at 250 Hz. The field at the end of the cylinder was 128 A/m@10 Hz. The frequency dependence of the internal field measured in the middle of the cylinder is shown in the Fig. 1. The field at the end decreases to 50 % at DC as theoretically predicted. This decrease is smaller for AC excitation as a consequence of the eddy currents; at 10 Hz the decrease is only 20 %.

FIG. 1 HERE

In order to optimize the direction and position of the fluxgate sensors and also to find the optimum excitation frequency we made extensive simulations based on FEM analysis. For the material properties we have used the following values: for the iron rod relative permeability $\mu = 50$ and conductivity $S = 10 \cdot 10^6$ S/m, for the aluminum cylinder and piston conductivity $S = 38 \cdot 10^6$ S/m Fig. 2 shows an example of the simulations: radial and axial field component calculated for four positions of the piston. The simulation shows that the field maximum is about 20 mm from the end of the bar and this distance is smaller at the limit position where the bar is completely out of the coil.

FIG. 2 HERE

The simulated reading of the sensors in positions A to D as the function of the piston position is shown in Fig. 3 for the frequencies from 2 Hz to 128 Hz.

The sensitivity decrease with frequency is caused by two effects:

1. eddy currents in the aluminum cylinder: the field from the excitation coil is attenuated by the shielding effect as shown in Fig. 1, and the response from the rod is attenuated again before it reaches the sensors. These two shielding factors are not the same, as in the first case the attenuated field is in the axial direction, while in the second case it is in the radial direction.

2. Eddy currents in the piston bar. They are also the main source of phase shifts.

The simulation show that the eddy currents in the aluminum piston give negligible contribution to the measured signal.

FIG. 3 HERE

The simulations were verified by measurement. An array of integrated fluxgate magnetic sensors was mounted in radial direction which is perpendicular to the primary field of the excitation coil. This was possible only because the used sensor has low crossfield error [10]. We have used integrated fluxgates DRV425 manufactured by Texas Instruments [11, 12]. The sensors were fixed in the plastic holders manufactured by 3-D printing. The experimental stand is shown in Fig. 4. The piston position was monitored by resistive transducer with 0.1 mm accuracy. The output voltage of the fluxgate sensors was measured by SR865 DSP Lock-in amplifier. The reference signal was derived from the coil current.

FIG. 4 HERE

In our case we used DRV425EVM modules with 0.5 mT range. However, using maximum range of 2 mT would allow to increase the excitation current by the factor of 10. In such case the noise limit would drop below 0.1 mm. The measured characteristics shown in Fig. 4. fits with the simulations. The sensitivity drops to one half at 20 Hz which is similar to the value predicted by simulations.

FIG. 5 HERE

Fig. 5 shows that the sensitivity in the radial direction is twice than the axial sensitivity. The axial field response is linear in the vicinity of the sensor location, which can be aslo used for the position sensing. The field in the axial direction was only 1.6 A/m. At 32 Hz the phase shift is large which makes modulus measurement of axial component useless. Regardless of using radial or axial field component. Sensor array should be used to cover strokes higher than 4 cm.

FIG. 6 HERE

III. Conclusion

Position of the piston in pneumatic cylinder can be measured by AC magnetic method. Using axial field excitation and an array of radially oriented fluxgate sensors on the cylinder surface an accuracy of 1 mm and resolution of 0.1 mm is achievable. The sensor linear range is 4 cm. For longer strokes

linear array of sensors spaced 2 to 3 cm should be used. The main advantages of the new method are:
1. it can be used on existing cylinders, both the coil and sensors are mounted outside the cylinder.
2. no influence of external magnetic fields
3. no need for expensive non-magnetic stainless steel piston rod.
4. resistance to the rod geometrical and magnetic imperfections (verified by measurement with several rods, some of them with a curvature and some of them exposed to mechanical shocks)

The disadvantage of the axial transducer is that the excitation frequency should be kept low, which limits the dynamic response of the transducer.

ACKNOWLEDGMENT

Andrey Chirtsov was supported by Texas Instrument.

REFERENCES

[1] I. Herceg: Taking a Position on Hydraulic Cylinder Sensors, Hydraulics & Pneumatics June 2015, 24-27
[2] Sorin Fericean, Andrea Hiller-Brod, Albert Daniel Dorneich, Markus Fritton, "Microwave Displacement Sensor for Hydraulic Devices", IEEE Sensors Journal, Vol. 13, No. 12, December 2013
[3] L. Shih-Yuan, L. Jyun and S. S. Lee, "The study of the piston driving and position sensing for a linearly moving piston pump," Automatic Control Conference (CACS), 2014 CACS International, Kaohsiung, 2014, pp. 287-291.
[4] K. Suzumori, J. Tanaka and T. Kanda, "Development of an intelligent pneumatic cylinder and its application to pneumatic servo mechanism," Proceedings, 2005 IEEE/ASME International Conference on Advanced Intelligent Mechatronics., Monterey, CA, 2005, pp. 479-484.
[5] A. A. M. Faudzi, K. Suzumori and S. Wakimoto, "Design and control of new intelligent pneumatic cylinder for intelligent chair tool application," 2009 IEEE/ASME International Conference on Advanced Intelligent Mechatronics, Singapore, 2009, pp. 1909-1914.
[6] Soon Yong Yang, Min Cheol Lee, Man Hyung Lee and S. Arimoto, "Measuring system for development of stroke-sensing cylinder for automatic excavator," in IEEE Transactions on Industrial Electronics, vol. 45, no. 3, pp. 376-384, Jun 1998.
[7] H. Sumali, E. P. Bystrom and G. W. Krutz, "A displacement sensor for nonmetallic hydraulic cylinders," in IEEE Sensors Journal, vol. 3, no. 6, pp. 818-826, Dec. 2003. doi: 10.1109/JSEN.2003.820333
[8] Y. Wang, R. Madson and R. Rajamani, "Nonlinear observer design for a magnetic position estimation technique," 2015 54th IEEE Conference on Decision and Control (CDC), Osaka, 2015, pp. 6986-6991.
[9] S. Taghvaeeyan R. Rajamani and Z. Sun (2013). Non-intrusive piston position measurement system using magnetic field. IEEE Sensors Journal, 13(8):3106–3114, 2013.
[10] P. Ripka, M. Janosek, M. Butta, S. W. Billingsley, E. Wakefield: Crossfield error in fluxgate and AMR sensors, Journal of Electrical Engineering. 2010, vol. 61, no. 7/s, p. 13-16.
[11] DRV425 Fluxgate Magnetic-Field Sensor, Texas Instruments datasheet at http://www.ti.com/product/DRV425/datasheet
[12] M. F. Snoeij, V. Schaffer, S. Udayashankar, Mikhail V. Ivanov: An Integrated Fluxgate Magnetometer for use in Closed-Loop/Open-Loop Isolated Current Sensing, IEEE J. Solid-state circuits 51 (2016), 1684-1694.

Appendix A

TABLE I
PARAMETERS OF THE EXCITATION COIL

Coil length (mm)	480		
Number of turns	808		
	DC	100 Hz	1 kHz
L (mH)	-	3,5	0,4
R (Ω)	14.1	15	18

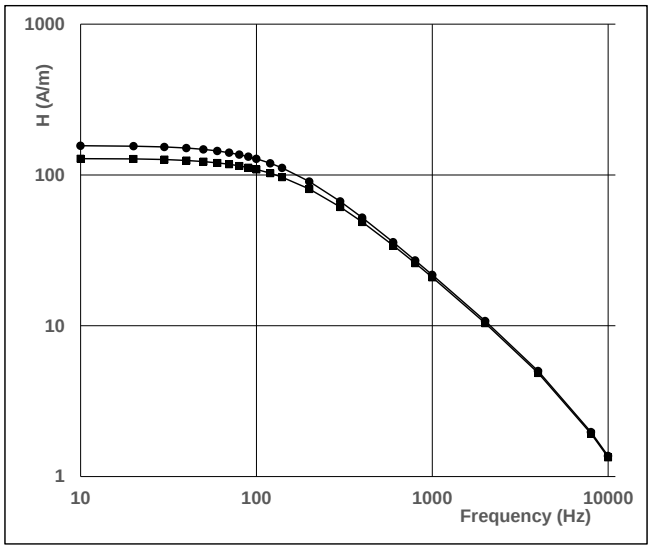

Fig. 1. Frequency dependence of the axial field in the middle of the cylinder (•) and at its ends (x)

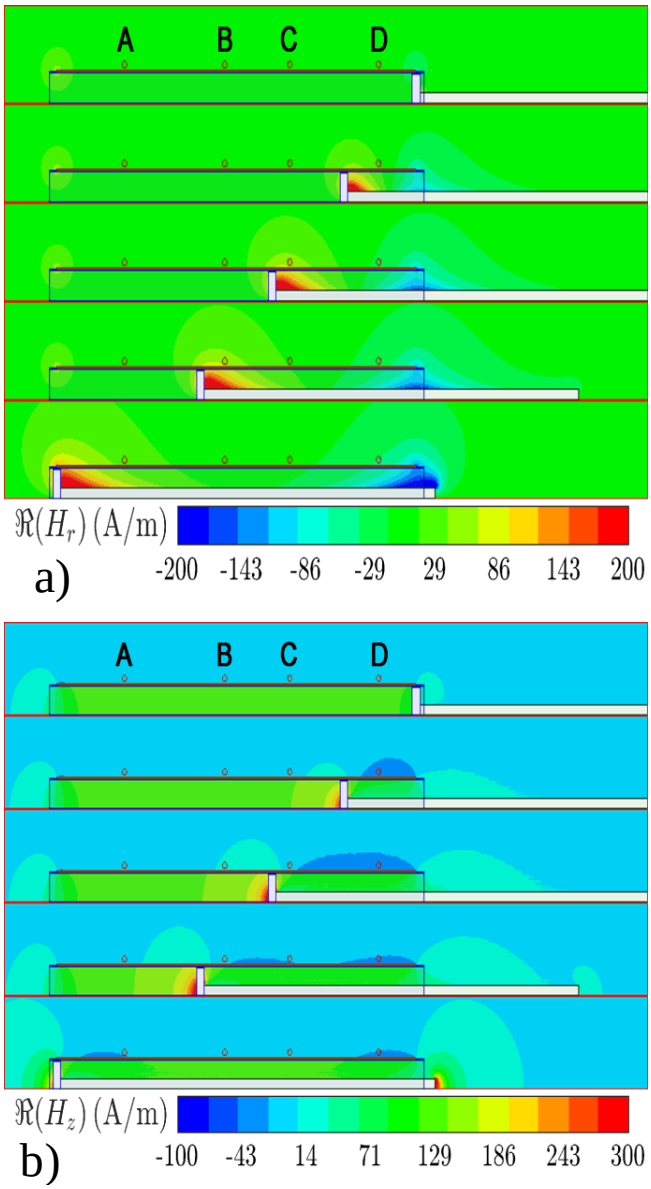

Fig. 2. FEM simulated field for several positions of the piston: a) radial component and b) axial component. The excitation frequency was 2 Hz. The location of the sensors is marked A to D.

Appendix A

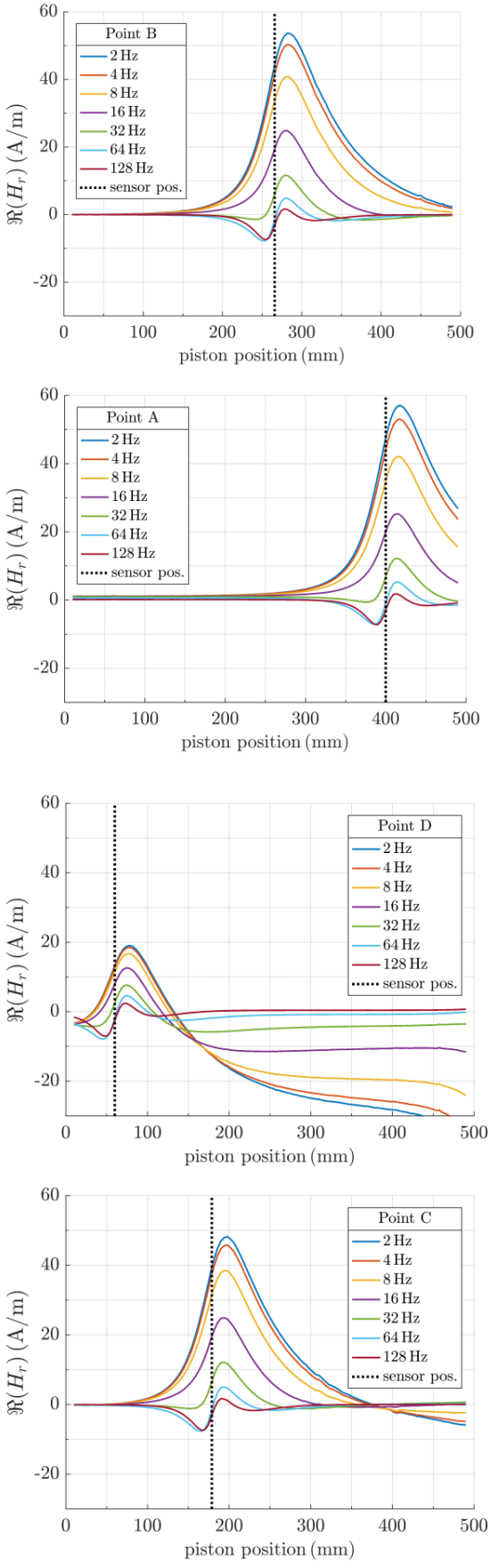

Fig. 3. : The reading of the sensors in positions A, C and D as the function of the piston position (FEM simulation)

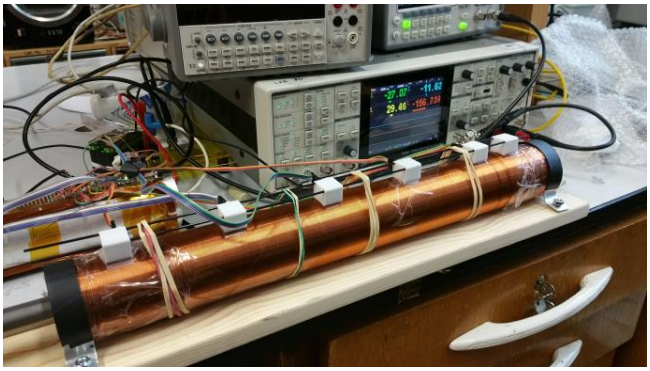

Fig. 4. : The reading of the sensors in positions B and C as the function of the piston position (measured X component)

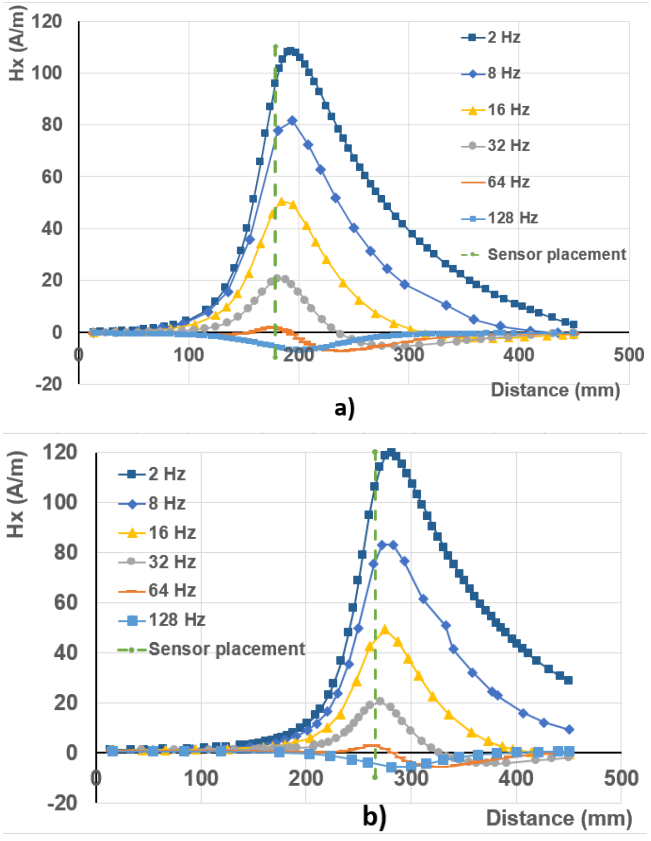

Fig. 5. : The reading of the sensors in positions B and C as the function of the piston position (measured X component)

Appendix A

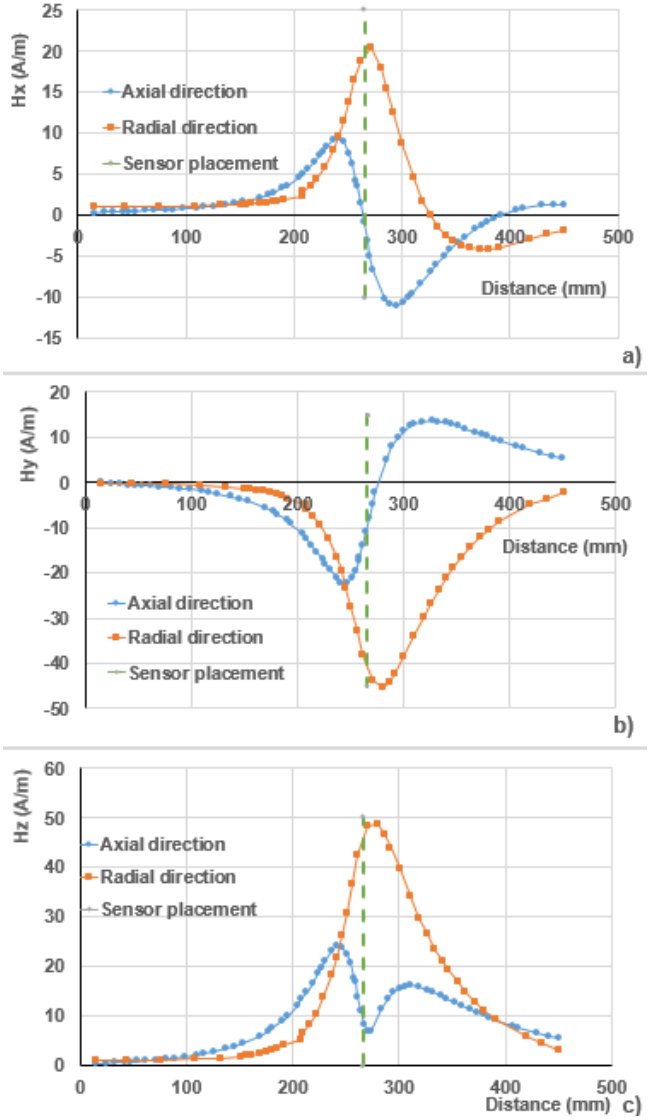

Fig. 6: Axial and radial field for 32 Hz excitation frequency a) X component (in-phase with current), b) Y component, c) modulus

Appendix A

Linear position sensing through conductive wall without permanent magnet

J. Vyhnanek[1], P. Ripka[1], A. Chirtsov[1]

1. Faculty of Electrical Engineering, Czech Technical University, Technicka 2, 166 27, Prague, Czech Republic

Summary

A linear position sensor for pneumatic actuators is presented. Position of the piston rod made of ferromagnetic material is detected by low frequency magnetic field which penetrates the aluminum wall of the cylinder. The sensor consists of an array of micro-fluxgates and two excitation saddle coils mounted outside the actuator. The method does not need a permanent magnet attached to the piston as required by common magnetic position sensors.

Motivation and results

The presented sensor is motivated by application of position sensing through conductive sheath presented in [1]. A low frequency magnetic field excitation penetrates thin conductive material and allows to detect metallic objects behind it. Active excitation allows synchronous demodulation of sensor signal to suppress off-band noise fields including DC. In the study ([1]) a 100 Hz excitation was used to detect position of objects through a 2.5 mm thick aluminum wall.

This method can be used for position detection of a piston in a pneumatic actuator which has usually an aluminum wall. So far for position sensing a permanent magnet had to be installed in the piston and a DC-field sensor detected its position [2]. Magnetic field of the permanent magnet then has to be strong enough to ensure good signal to noise ratio to suppress DC field noise.

The proposed sensor does not need modifications to the piston, it is installed externally on the actuator wall (Fig. 1). The magnetic field response of the steel rod to the radial excitation field is sensed by micro-fluxgate sensors in axial direction. The response is frequency dependent. At very low frequencies only permeability effects contribute to the signal, at 64 Hz eddy current effects change noticeably the shape of characteristics (Fig. 2). The selection of the used excitation frequency depends on the required dynamic properties of the designed sensor. We evaluated the error of position measurement with excitation frequency of 32 Hz and 16 sensors in the array with 3-cm spacing (Fig. 3). Using least mean squares fitting method the positioning error is below ±2 mm throughout the central 300 mm stroke of the 500 mm long pneumatic actuator. This is initial accuracy achieved without any corrections.

Due to the low amplitude of the signal measured, which is about 1/1000 of the amplitude provided by a piston magnet, the position sensor is susceptible to the background magnetic noise. Methods of noise suppression which does not compromise the sensor frequency response will be evaluated in the full paper.

Word count: 408

References

[1] P. Ripka, J. Vyhnanek, M. Janosek, J. Vcelak (2014): AMR Proximity Sensor With Inherent Demodulation. *IEEE Sens J* **9**, 3119-3123.

[2] T. Reininger, F. Welker, M. von Zeppelin (2006): Sensors in position control applications for industrial automation. *Sens Act A: Phys* **129**, 270-274.

Corresponding author

Jan Vyhnanek, Faculty of Electrical Engineering, Czech Technical University, Technicka 2, 166 27, Prague, +420-22435-2178, vyhnajan@fel.cvut.cz

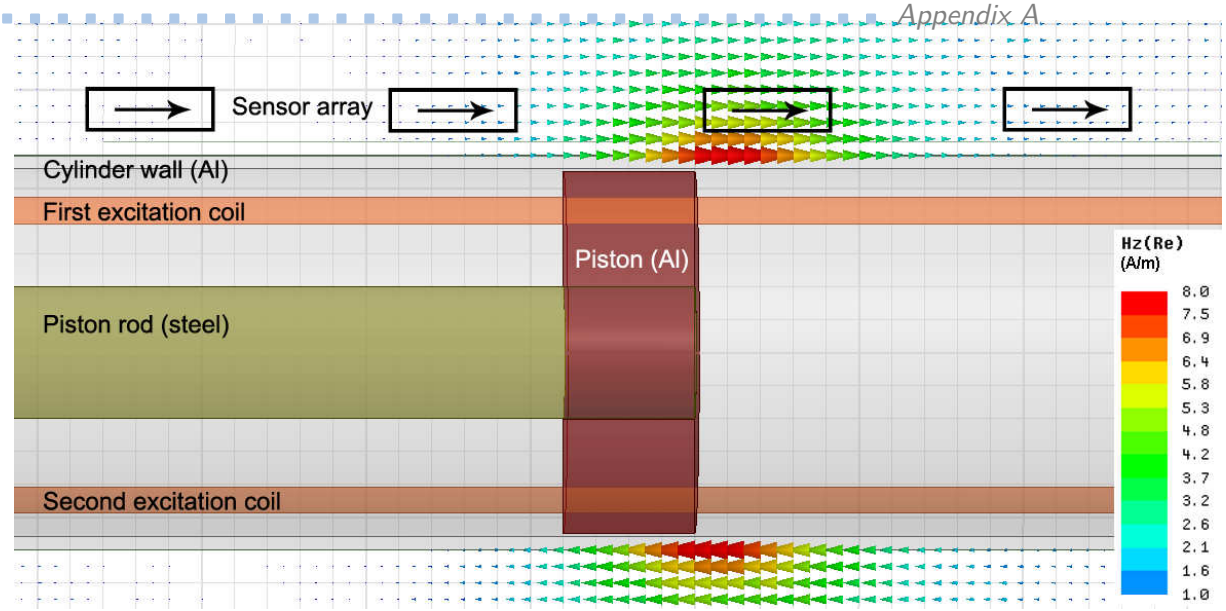

Figure 1: Magnetic field component in axial direction outside a pneumatic cylinder 6 cm in diameter simulated by FEM. Excitation field of 4 Hz in radial direction penetrates the aluminum wall and is substantially deformed near the end of the piston rod made of common magnetizable steel. Sensors are oriented in the axial direction and perpendicularly to the excitation field.

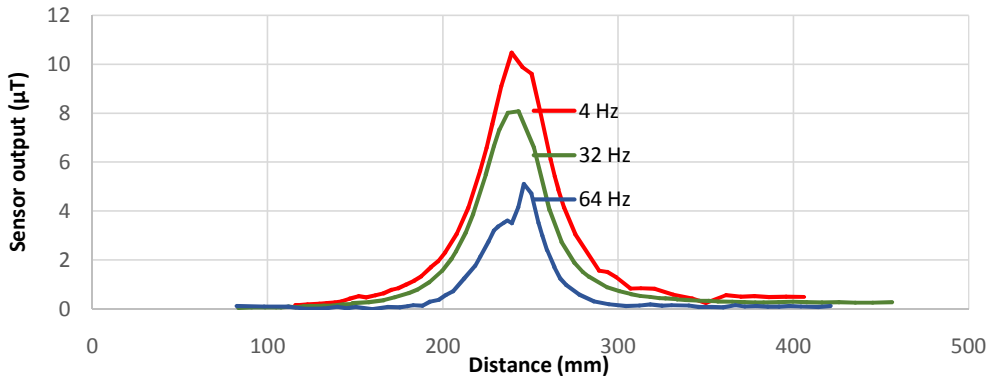

Figure 2: Single sensor output vs. piston position for excitation frequency of 4 Hz, 32 Hz and 64 Hz .

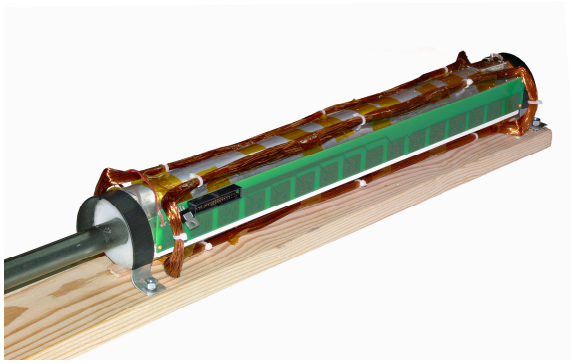

Figure 3: The position sensor made of 16 integrated fluxgate sensors and two excitation saddle coils is attached to the pneumatic actuator model.